https://doi.org/10.5194/egusphere-2025-5625
Preprint. Discussion started: 20 January 2026

Enhancing hydrological representation of the Brahmaputra basin through terrestrial water storage and surface soil moisture Data Assimilation

Leire Retegui-Schiettekatte[1,2], Manuela Girotto[2], Maike Schumacher[1], Mohammad Shamsudduha[3], Henrik Madsen[4], and Ehsan Forootan[1,5]

[1]Geodesy Group, Department of Sustainability and Planning, Aalborg University, Rendsburggade 14, Aalborg, 9000, Denmark
[2]University of California Berkeley, Berkeley, CA, United States
[3]Department of Risk and Disaster Reduction, University College London, Gower Street, London, WC1E 6BT, United Kingdom
[4]DHI A/S, Agern Allé 5, Hørsholm, 2970, Denmark
[5]School of Geographical Sciences, University of Bristol, University Rd, Bristol BS8 1SS, United Kingdom

Correspondence: Leire Retegui-Schiettekatte (leirears@plan.aau.dk)

Abstract. Understanding the dynamics of terrestrial water storage (TWS), and its components such as surface soil moisture (SSM) and groundwater, is important for the Brahmaputra River Basin, where water resources are expected to experience increasing demand and are highly vulnerable to extreme hydrological events and climate change. However, water storage dynamics are complex and difficult to capture by state-of-the-art large-scale hydrological models. In this study, we implement a multi-variate daily TWS and daily SSM sequential Data Assimilation (DA) with the aim of improving model-derived water storage dynamics. In our methodology, we propose a model space covariance localization approach that is compared with three other approaches used in the previous literature. The results show that this new approach is the only one to effectively mitigate cross-variable influences along the vertical water storage profile, which have been reported as one of the main challenges of multi-variate land DA. A validation of the multi-variate DA estimates (for the period 2004-2015) indicates that more realistic decadal trend and inter-annual variability are introduced into the groundwater estimates, increasing the correlation coefficients with the Standardized Precipitation Evapotranspiration Index and observed groundwater levels by +0.24 to +0.54 correlation points. With respect to SSM, DA induces a general phase shift, especially around mountain areas. Improved land water storage estimates reveal a land water decline of 70.9 GT per decade for the period 2004-2015 in the Brahmaputra River basin, which constitutes approximately half of the TWS decline in that period, with the other half caused by glacier retreat (67.5 GT per decade).

Short summary: An improved method is used to integrate satellite-derived terrestrial water storage and surface soil moisture observations into a hydrological model within the Brahmaputra River basin (South Asia). This integration leads to a more realistic representation of the water stored in the land, allowing us to better understand its changes in space and time, which is crucial in this basin due to its increasing water demand and vulnerability to extreme events due to climate change.

https://doi.org/10.5194/egusphere-2025-5625
Preprint. Discussion started: 20 January 2026

1 Introduction

Due to population growth and urban and industrial development, as well as climate change, water availability and security in the Brahmaputra River Basin are becoming more uncertain (Das and Kumar, 2019). On the one hand, demographic and economic growth, accompanied by consequent changes in land use, can lead to a higher water demand, potentially resulting in regional water scarcity (Gain and Wada, 2014; Kirby and Mainuddin, 2022). Groundwater depletion has already been detected related to agricultural and urban water use (for example, in northwestern Bangladesh, a region adjacent to the Brahmaputra basin, or around the city of Dhaka in the southern part of the Brahmaputra basin) (Shamsudduha et al., 2012, computed over period 1985-2007). On the other hand, the IPCC report (Intergovernmental Panel On Climate Change (IPCC), 2023) states that climate change, through changes in precipitation patterns (Gogoi et al., 2023), glacier melting and snow melting (Lutz et al., 2014; Nie et al., 2021), is likely to cause increased extreme river flows in the Brahmaputra River, further enhancing flooding events (Gain et al., 2011; Masood et al., 2015; Dutta et al., 2021; Alam et al., 2021). In addition, sea-level rise also poses higher flood risks for coastal areas (Brown et al., 2018; Rahman et al., 2019). These events can cause enormous human and economic damage and threaten the water security of the region (Das and Kumar, 2019; Kirby and Mainuddin, 2022).

Effective management of water resources and mitigation of risks posed by extreme events require a clear understanding of spatial and temporal changes in the variability of land water storage (that is, groundwater and soil water). This knowledge is essential to plan and implement water conservation measures, especially in the face of climate change (Sammonds et al., 2021). Hydrological models are the main tool to simulate and predict water variability; however, their performance is limited due to many factors such as the complexity of hydrological processes, limited in situ data for performing calibrations, and the uncertainty of input climate forcing fields (Kauffeldt et al., 2016; Mehrnegar et al., 2020).

Satellite Earth Observation (EO) can be used to monitor various aspects of the global water cycle (Dube et al., 2023) and are especially useful in poorly gauged or ungauged basins. Measurements provided by the Gravity Recovery and Climate Experiment (GRACE, Tapley et al., 2004) and its Follow-On mission (GRACE-FO, Flechtner et al., 2014) can be used to detect time-variable changes in terrestrial water storage (TWS), which represent the total amount of water on Earth's land surface and in the subsurface, encompassing components such as groundwater, soil moisture, lakes, rivers, snowpack, and glaciers. Changes in TWS reflect the net effect of natural processes and anthropogenic modifications on the available water budget (Eicker et al., 2016; Kusche et al., 2016). Remotely sensed surface soil moisture (SSM) is an important EO product, which represents the water stored in the first few centimeters of the Earth's surface (Kerr et al., 2010; Entekhabi et al., 2010). Satellite missions such as SMOS, SMAP, Sentinel-1, and MetOp have been used in the past to retrieve SSM products globally.

Although satellite-based observations provide very useful information, their performance is limited to low spatial-temporal resolutions: for example, GRACE-FO is resolved monthly with ~ 300 km resolution or daily with ~ 450 km resolution, while SSM can be few-daily with 1-25 km spatial resolution. Additionally, temporal gaps can be found in the data series due to sensor or orbital instability (mainly in TWS), as well as difficult retrieval conditions (in SSM), and uncertainties in retrieval algorithms may cause biases (Gruber et al., 2020; Yang et al., 2024). Furthermore, each EO product only provides information on a particular variable of the water cycle while, in contrast, models simulate various water storage and flux components, as

https://doi.org/10.5194/egusphere-2025-5625
Preprint. Discussion started: 20 January 2026

well as their interactions. Hence, a logical step is to integrate EOs into models to combine their advantages, which can be pursued through data-model fusion frameworks.

The ensemble-based sequential Data Assimilation (DA) is a popular approach to perform data-model fusion in hydrological applications (Reichle, 2008). These DA frameworks allow us to integrate various observations, when they are available, within the model while accounting for the uncertainty of both the model and the observations. The assimilation of monthly GRACE TWS in hydrological models has been applied globally (Li et al., 2019; Gerdener et al., 2023; Yang et al., 2025) and within various river basins. The TWS DA has been found to improve the TWS and groundwater dynamics of models, by correcting trend, seasonal, and inter-annual variability (Zaitchik et al., 2008; Van Dijk et al., 2014; Girotto et al., 2016, 2017; Schumacher et al., 2018; Getirana et al., 2020; Bolaños Chavarría et al., 2022; Schumacher et al., 2025). Generally speaking, the product of TWS DA presents the realism of GRACE(-FO) TWS observations while preserving the finer spatial resolution and individual water storage and flux estimates of hydrological models (Yang et al., 2025) and allows to compute the water storage variability of individual water storage components with a better accuracy than simpler component reduction methods (Getirana et al., 2025). However, one of the main challenges reported in the TWS DA is the vertical disaggregation of storage updates, which can degrade SSM estimates (Girotto et al., 2016, 2019; Tangdamrongsub et al., 2020; Retegui-Schiettekatte et al., 2025a).

Various studies have also assimilated SSM retrievals into different hydrological models (e.g., Reichle and Koster, 2005; Crow and Ryu, 2009; Brocca et al., 2010; Renzullo et al., 2014; Ridler et al., 2014; Massari et al., 2015; Blyverket et al., 2019; De Lannoy et al., 2024). Some of them reported notable improvements in near-surface soil moisture and root-zone water storage estimations, as well as a better representation of hydrological fluxes such as runoff (Brocca et al., 2010; Massari et al., 2015; De Lannoy et al., 2024). Nevertheless, SSM DA has also been found to (partially) degrade deeper soil water, groundwater and TWS estimates (Ridler et al., 2014; Tian et al., 2017; Girotto et al., 2019) and have a neutral or negative impact on river runoff estimates (Chen et al., 2011; Matgen et al., 2012; Ridler et al., 2014).

A strategy to address the complementary issues of TWS DA and SSM DA can be realized by simultaneously assimilating both observations (multi-variate DA). Table 1 provides an overview of the existing literature on multivariate TWS and SSM DA and their DA techniques, as well as their main findings. These multivariate experiments were found to improve both SSM and groundwater components (Tian et al., 2017; Girotto et al., 2019; Khaki et al., 2019; Khaki and Awange, 2019; Khaki et al., 2020; Tangdamrongsub et al., 2020) and indirectly modify other water balance components such as snow, streamflow, and evapotranspiration (Zhao and Yang, 2018; Wu et al., 2022; Wongchuig et al., 2024).

Nevertheless, the multi-variate DA still presents challenges that remain unsolved. Namely, previous studies reported conflicts between TWS and SSM observations that, to different extents, diminish the improvement of model estimates in the multi-variate implementation compared to a uni-variate implementation (Tian et al., 2017; Zhao and Yang, 2018; Girotto et al., 2019; Tangdamrongsub et al., 2020; Wongchuig et al., 2024). This cross-variable interference is not necessarily a problem and has been found to lead to enhanced estimates in some cases (Khaki et al., 2019; Khaki and Awange, 2019; Khaki et al., 2020). However, Girotto et al. (2019) showed that when the updates introduced by the different observations are anti-correlated, they can end up canceling each other. Furthermore, in some of these studies, the success of the DA experiment is found to be

https://doi.org/10.5194/egusphere-2025-5625
Preprint. Discussion started: 20 January 2026

conditioned by an appropriate adjustment of observation uncertainties, which should be estimated heuristically (Tian et al., 2017). So far, there have been no clear studies or guidelines on how to appropriately address these issues.

In this study, satellite-derived TWS and SSM are assimilated into a hydrological model in the Brahmaputra River basin. The study pursues two main objectives: (i) to explore how different multi-variate TWS and SSM DA settings can generate or avoid some of the issues reported in previous literature, and (ii) to produce improved land water storage estimates and to draw insights on its spatial and temporal variability for the Brahmaputra River basin. To reach the first objective, we test different DA settings and propose a novel approach, here called "model space mixed localization", to maximize the performance of the multi-variate DA. Regarding the second objective, we first validate the multivariate DA estimates against independent in situ streamflow and groundwater data, as well as the Standardized Precipitation Evapotranspiration Index (SPEI) and SSM estimates from an independent model. Finally, we analyze the decadal, inter-annual and seasonal variability of land water storage in the region.

The paper is organized as follows: first, the study area, data and model, method and experimental setting are introduced; second, evaluation, validation, and interpretation of the results are presented and discussed; finally, concluding remarks close the paper.

https://doi.org/10.5194/egusphere-2025-5625
Preprint. Discussion started: 20 January 2026

	Tian et al. (2017)	**Zhao & Yang (2018); Wu et al. (2022)**	**Khaki & Awange (2019); Khaki et al. (2019, 2020)**	**Girotto et al. (2019)**	**Tangdamrongsub et al. (2020)**	**Wongchuig et al. (2024)**
Model	W3	CLM4	W3RA	CLSM	CABLE	MGB
Region and period	Australia 2010-2013	Global 2003-2009	South America 2002-2013 // Mississippi and Murray-Darling basin, 2003-2012	US 2010-2016	Goulburn River catchment (Australia) 2010-2016	Amazon River basin 2000-2020
Assimilated obs.	-Monthly GRACE TWS -SMOS SSM	-Daily GRACE TWS -AMSR-E bightness temperature -MODIS snow cover fraction	-5-daily GRACE TWS -5-daily SMOS and AMSR-E SSM (-AVHRR Leaf Area Index)	-Monthly GRACE TWS -SMOS brightness temperature	-Monhtly GRACE TWS -SMOS and SMAP SSM	-5-daily GRACE TWS -ASCAT, SMOS, SMAP and AMSR-E SSM -Altimetric water surface elevation -Satellite -derived flood extent
DA technique	EnKS	EAKF	EnSRF, UW-CEnKF, SQRA, Kalman-Takens	2-step EnKF	2-step EnKS	EnKF
Localization/ Additional adjustments	-Obs. uncertainty adjustment -No localization reported	-Obs. space uniform covariance localization: $\sim 3^\circ$ for all obs.	-Obs. uncertainty adjustment -Obs. space uniform covariance localization: $\sim 3^\circ$ for all obs.	-Obs. space mixed covariance localization: 6° for TWS, 1° for brightness temperature	- Obs. space mixed covariance localization: whole study area for TWS, $\sim 0.25^\circ$ for SSM	-Obs. space mixed covariance localization: $\sim 5^\circ - 10^\circ$ for TWS, smaller for SSM, adapted to physical catchment characteristics
Reported achievements	Improved SSM, groundwater and streamflow; temporal downscaling through smoother approach.	Improved SSM and snow; improved discharge for some basins	Improved groundwater and SSM; multi-variate DA generates larger improvements wrt uni-variate DA	Improved SSM, groundwater and runoff	Improved SSM and groundwater	Improved streamflow and evapotranspiration
Reported limitations	Reduced impact of multi-variate DA wrt uni-variate DA for SSM, TWS, evapotranspiration and streamflow	TWS DA dominates over SSM in multi-variate experiment		Reduced impact of multi-variate DA wrt uni-variate DA for rootzone soil moisture, surface soil moisture (to some extent) and runoff	Reduced impact of multi-variate DA wrt uni-variate DA for SSM and groundwater	Reduced impact of multi-variate DA wrt uni-variate DA for streamflow and evapotranspiration

Table 1. Summary of experimental setting and main result of previous multi-variate land DA experiments involving TWS and SSM data. "wrt" = with respect to; "obs" = observation(s). The abbreviations in "DA techniques" (row 4) refer to the Ensemble Kalman Filter (EnKF), Ensemble Kalman Smoother (EnKS), Ensemble Adjustment Kalman Filter (EAKF), Ensemble Square Root Filter (EnSRF), Unsupervised Weak Constrained Ensemble Kalman Filter (UWCEnKF) and Square Root Analysis (SQRA). More details on localization and DA adjustment approaches (row 5) is provided in Section 2.3.3

https://doi.org/10.5194/egusphere-2025-5625
Preprint. Discussion started: 20 January 2026

2 Study area, data and method

2.1 Study area

The Brahmaputra River basin, one of the largest river basins in the world, has a drainage area of about 530,000 km^2 (which covers China, India, Bangladesh, and Bhutan). The hydrology of the basin is characterized by a strong seasonality caused by monsoonal precipitation, with a wet season from June to September accounting for 60 to 70 % of its annual rainfall (Immerzeel, 2008). This results in a rapid saturation of the soil around June, which is typically sustained during the wet period. Groundwater also presents a strong seasonality as it is largely recharged through rainfall and river flow infiltration processes in the monsoon season (Medhi et al., 2024; Shamsudduha et al., 2022).

The Brahmaputra River produces an average discharge of approximately 20,000 m^3 s^{-1}. In the upper stage of the river, glacier and snow melt are estimated to contribute approximately 20-25 % of river discharge, while rainfall runoff dominates with 59 % of contribution (Lutz et al., 2014; Chen et al., 2017). Floods are common during the wet season in southern agricultural floodplains and often cause huge socio-economical impacts, including large fatalities, the displacement of thousands of people, and damage to crops resulting in famine (Brammer, 1990; Mirza, 2003). The river flow regime is expected to change with climate change: glaciers in the area have been reported to retreat by approximately -0.5 m of water equivalent per year for the period 2000-2018/9 (Shean et al., 2020; Hugonnet et al., 2021; Vishwakarma et al., 2022), and are likely to further retreat in the next few decades (Lutz et al., 2014; Nie et al., 2021). This is expected to generate higher flows during the monsoon period, increasing the risk of flooding and posing a threat to the livelihoods and food and water security of the area (Intergovernmental Panel On Climate Change (IPCC), 2023; Uhe et al., 2019; Dutta et al., 2021; Alam et al., 2021).

The communities along the Brahmaputra River basin depend on these water resources for agriculture and domestic use. Approximately 25 % of the Brahmaputra River Basin is classified as agricultural land (Commission, 2014), with a particularly high presence of irrigation in Bangladesh (Siebert et al., 2013). Although surface water is abundant during the monsoon season, it can become scarce during the dry season, increasing the need for groundwater abstraction for agricultural irrigation (Shamsudduha and Panda, 2019). Estimates for October 2013 suggest that the groundwater-fed irrigation exceeds surface water-fed irrigation in many parts of the basin (Siebert et al., 2013). Groundwater storage declines of -2 to -5 cm per year due to agricultural abstraction have been reported in the northwest of Bangladesh (region adjacent to the Brahmaputra River basin). In addition, similar-sized declines in groundwater have also been reported around the capital city of Bangladesh, Dhaka (Shamsudduha et al., 2012). In the rest of the basin (that is, the East and West sub-basins of this study), the anthropogenic impact on land water resources is considered limited (Khandu et al., 2016; Maina et al., 2024).

In addition to the Brahmaputra River basin, the DA area in this study also includes the Meghna River basin (drainage area of approximately 82,000 km^2) as well as the confluence of the Brahmaputra, Ganges, and Meghna Rivers. As the two latter only contribute in the South sub-basin (Fig. 1), and for the sake of conciseness, in this study the whole area is generically referred to as the Brahmaputra River basin. For the assimilation of TWS and interpretation of the results, the basin was divided into the East, West and South sub-basins (Fig. 1).

https://doi.org/10.5194/egusphere-2025-5625
Preprint. Discussion started: 20 January 2026

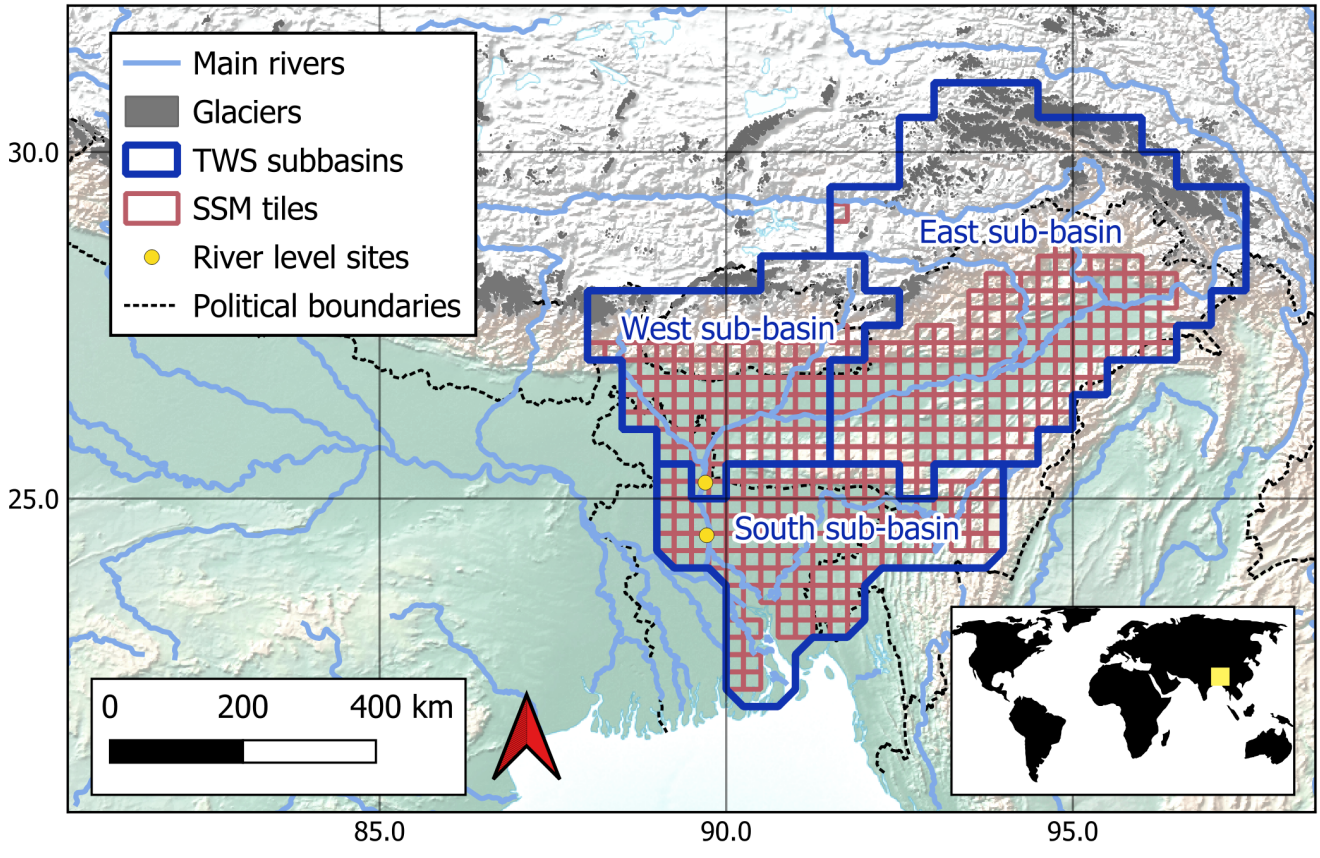

Figure 1. An overview of the Brahmaputra River basin with the three sub-basins (with areas of 253,000, 105,000, and 107,000 km^2), in which TWS is assimilated (blue boundaries). The red grid boxes ($0.25° \times 0.25°$) represent the locations where the ESA CCI SSM products are assimilated.

2.2 Data and model

Model

This study uses the World Wide Water Resources Assessment model (W3RA, van Dijk, 2010; van Dijk et al., 2013) with a spatial resolution of $0.1° \times 0.1°$ (approximately 10 km $\times$ 10 km) and a daily temporal resolution. The model was forced by precipitation, maximum and minimum temperature, and downward surface solar radiation data derived from ERA5 (Hersbach and Dee, 2016) and ERA5-Land (Muñoz Sabater et al., 2019) (see more details in Section 3.1). The model has four different land water storage components: topsoil, shallow soil, deep soil, and groundwater (Table 2). In each grid cell, the topsoil, shallow soil and deep soil components are distinctly estimated for two hydrological response units: one corresponding to short shallow-rooted vegetation cover, and one corresponding to tall deep-rooted vegetation cover. In this study, topsoil and shallow soil are

https://doi.org/10.5194/egusphere-2025-5625
Preprint. Discussion started: 20 January 2026

treated jointly as "SSM", and deep soil and groundwater are treated jointly as "groundwater" (a detailed explanation of the reason behind this aggregation is provided in Section 3.1). Additionally, the model also accounts for processes involving runoff generation, vegetation, and snowpack, but it does not have a glacier simulation module. In this study, W3RA was coupled with a grid-based river routing model (Mizukami et al., 2016) for the calculation of river water storage.

	Conceptual extent	**Average field capacity over study area**
Topsoil ($S0$)	First few centimeters under soil surface.	67 mm
Shallow soil (Ss)	Soil layer to which both short (shallow-rooted) and tall (deep-rooted) vegetation have access for water uptake.	27 mm
Deep soil (Sd)	Soil layer to which only tall (deep-rooted) vegetation has access for water uptake.	358 mm
Groundwater (Sg)	Groundwater (no vegetation water uptake).	- no maximum field capacity -

Table 2. Overview of W3RA land water storage compartments and their respective field capacities in the study area.

Assimilated data

The daily TWS was derived from the daily GRACE products of ITSG-2018 (Mayer-Gürr et al., 2018; Kvas et al., 2019). The daily product was chosen over traditional monthly GRACE products for two reasons: (i) to avoid the temporal mismatch between TWS and SSM observations, as well as with the model; and (ii) to improve the model TWS estimates on the sub-seasonal and sub-monthly timescales (Retegui-Schiettekatte et al., 2025a). In this study, we only considered data for the period 2003-2015 to limit the temporal extent of each experiment (and hence their computational cost) and to avoid having to deal with the gap between GRACE and GRACE-FO missions (2017-2018). The post-processing applied to the data included recommended spherical harmonic corrections, geophysical inversion, and leakage error correction (see more details in Retegui-Schiettekatte et al., 2025a; Mehrnegar and Forootan, 2025). The time-dependent error variance of the spherical harmonics was post-processed accordingly and rescaled at the end of the process to fit the values reported in Boergens et al. (2022).

The daily SSM estimates originate from the European Space Agency Climate Change Initiative (ESA CCI) Combined SSM product (v08.1) (Gruber et al., 2019; Dorigo et al., 2017; Preimesberger et al., 2021). This dataset was chosen because of its daily sampling, avoiding a temporal mismatch with the model. The combined product merges SSM retrievals derived from various active and passive satellite sensors and is provided on $0.25° \times 0.25°$ tiles (Fig. 1), with uncertainties computed using a triple-collocation technique. The merging process includes rescaling the retrievals to a common baseline (modeled soil moisture of GLDAS Noah, Gruber et al., 2019). To avoid mismatches with our model, before performing DA, we re-rescaled the ESA CCI SSM estimates to the range of W3RA SSM estimates (see more details in Section 3.1).

Validation data

In situ groundwater level observations and river water level observations of the Bangladesh Water Development Board (BWDB) (see Shamsudduha et al., 2012, 2022), available in the area of Bangladesh, have been used for validation. 263 ground-

https://doi.org/10.5194/egusphere-2025-5625
Preprint. Discussion started: 20 January 2026

water observation sites were available for the study area, located mainly in the South sub-basin and covering the entire study period (Fig. 7). Regarding river level observation sites, a selection was carried out according to the following criteria: (i) the sites should be located on the main branch of the Brahmaputra River; and (ii) they should be as close as possible to the sub-basin outlets, to reflect the impact of sub-basin averaged TWS assimilation on river water levels. Two sites were selected for the West and South sub-basins (Fig. 1), which provide data for the entire study period with few temporal gaps (Fig. 9). No river observation site was available for the East sub-basin.

The Standardized Precipitation Evapotranspiration Index (SPEI, Vicente-Serrano et al., 2010) aggregated over a 12-month time window (SPEI-12) is used as an indicator of hydrological dryness-wetness conditions. The SPEI-12 time series for each sub-basin were derived from the Global Drought Monitor (Beguería et al., 2014) and are used to validate the inter-annual groundwater dynamics.

TWS in the East and West sub-basins is affected by trends caused by glacier retreat (Wouters et al., 2019; Sherpa and Werth, 2025). In this study, glacier trends are removed after the DA experiment from the model groundwater estimates. Glacier retreat data are taken from three previous studies based on satellite stereo imagery (Brun et al., 2017; Shean et al., 2020; Hugonnet et al., 2021). The Randolph Glacier Inventory 7.0 dataset (RGI Consortium, 2023) was used to compute the total area covered by glaciers in each sub-basin, resulting in 7719 km^2 and 3406 km^2 for the East and West sub-basins, respectively.

An independent validation of SSM is not straightforward because (i) there is no in-situ SSM observation openly available in the study region; and (ii) various active and passive satellite SSM retrievals are included in the assimilated ESA CCI Combined SSM, and therefore a comparison against any of these SSM products cannot be considered independent. Due to these limitations, SSM estimates are evaluated against soil water storage estimates from the WaterGAP global hydrology and water use model (Döll et al., 2003; Müller Schmied et al., 2024; Nyenah et al., 2025), which are resolved with daily and $0.5° \times 0.5°$ resolution. A 10 km resolution topographic slope dataset was used to support the interpretation of spatial SSM difference patterns (Amatulli et al., 2018).

2.3 Method

2.3.1 Data Assimilation

Following previous literature on land DA (Girotto et al., 2019; Tangdamrongsub et al., 2022; Wongchuig et al., 2024), DA was performed using an Ensemble Kalman Filter (EnKF) approach (Evensen, 1994; Houtekamer and Mitchell, 1998; Evensen, 2003). The EnKF is a Monte-Carlo approach in which the uncertainty of the model is computed through an ensemble run of N_e perturbed model realization (more details on the perturbation method can be found in Section 3.1). The objective here is to update the ensemble of model states ($X_k = [x_k^{(1)}, x_k^{(2)}, ..., x_k^{(N_e)}]$) for every timestep k, where the model state $x_k^{(i)}$ represents the water storage values predicted by the model for each grid cell and each water storage component in that timestep. The updated model state for the timestep k is computed as

$$X_k^+ = X_k^- + K_k(Y_k^o - AX_k^-), \tag{1}$$

https://doi.org/10.5194/egusphere-2025-5625
Preprint. Discussion started: 20 January 2026

where X_k^- is the predicted model state ensemble matrix for the timestep k, which contains, in its column i, the model state of the i^{th} ensemble member, and X_k^+ is the updated model state ensemble matrix for the same timestep, with a similar structure. The observation matrix Y_k^o contains each i^{th} perturbed set of observation (here TWS, SSM or both) in its i^{th} column. These observations are perturbed according to their uncertainty, in order to guaranty a realistic ensemble spread in the updated model states (Burgers et al., 1998, see more information on the perturbation method in Section 3.1). The matrix A is the forward observation operator that, when applied to the model state, generates the observation prediction. K_k is the Kalman gain matrix, which is defined as

$$K_k = C(X_k^-)A^\top (AC(X_k^-)A^\top + \Sigma_{y^o,k})^{-1}. \tag{2}$$

$\Sigma_{y^o,k}$ refers to the error covariance matrix of the observations. $C(X_k^-)$ is the ensemble-based error covariance matrix of the model state and is computed as $C(X_k) = \frac{1}{N_e-1}\Delta X_k \Delta X_k^\top$, where the matrix ΔX_k contains, in its i^{th} column, the deviation of the ensemble member i from the ensemble-average of the model state, $x_k^{(i)} - \frac{1}{N_e}\sum_{i=1}^{N_e} x_k^{(i)}$.

2.3.2 Uni-variate and multi-variate DA

In the uni-variate (i.e., single-observation) TWS DA experiment, $Y^0_{k,TWS}$ and $\Sigma_{y^o_{TWS},k}$ are used within the EnKF equations, which represent the perturbed TWS observations and their uncertainty, respectively. The forward TWS computation operator, A_{TWS}, vertically aggregates all water storage compartments and horizontally averages gridded model estimates on three sub-basins (Fig. 1). For the uni-variate SSM DA experiment, $Y^0_{k,SSM}$ and $\Sigma_{y^o_{SSM},k}$ represent the perturbed SSM observations and their uncertainty, respectively. The forward SSM computation operator (A_{SSM}) aggregates the water storage components corresponding to SSM and averages gridded model estimates on the $0.25° \times 0.25°$ ESA CCI tiles (Fig. 1).

Multi-variate DA can be implemented in a similar way to uni-variate DA by extending the observation matrix to include all observations in the following way (Wongchuig et al., 2024)

$$Y^o_{k,multi-variate} = \begin{pmatrix} Y^o_{k,TWS} \\ Y^o_{k,SSM} \end{pmatrix}. \tag{3}$$

The observation error covariance matrix and the forward operator matrix also need to be updated accordingly, that is, $\Sigma_{y^o_{multi-variate},k} = \begin{pmatrix} \Sigma_{y^o_{TWS},k} & 0 \\ 0 & \Sigma_{y^o_{SSM},k} \end{pmatrix}$ and $A_{multi-variate} = \begin{pmatrix} A_{TWS} \\ A_{SSM} \end{pmatrix}$.

Previous studies by Tian et al. (2017); Girotto et al. (2019); Tangdamrongsub et al. (2020) include two-step update schemes or temporal smoothers to address the temporal mismatch issue between the model and observations. These approaches are not necessary in this study, as both observations are assimilated in the same daily timescale as the model. This implies that the forward observation operator matrices $A_{TWS/SSM/multi-variate}$ here perform a vertical aggregation and horizontal averaging, but do not apply any temporal averaging.

https://doi.org/10.5194/egusphere-2025-5625
Preprint. Discussion started: 20 January 2026

2.3.3 DA tuning approaches

Most of the previous TWS and SSM DA experiments shared a similar EnKF update framework, but tuned the DA implementation differently (see Table 1). In this paper, we study the impact of two of these tuning approaches: uncertainty adjustment and covariance localization.

Uncertainty adjustment

The uncertainty adjustment (see, e.g., Tian et al., 2017) is implemented to achieve a better balance between the TWS and SSM observations, and to avoid that one observation type dominates over the other. It consists of multiplying the TWS and SSM observation uncertainties with scaling factors (α_{TWS} and α_{SSM}, respectively), which must be set heuristically (see more details in Section 3.1),

$$\Sigma^{adjusted}_{y^o_{multi-variate},k} = \begin{pmatrix} (\alpha_{TWS})^2 \cdot \Sigma_{TWS,k} & 0 \\ 0 & (\alpha_{SSM})^2 \cdot \Sigma_{SSM,k} \end{pmatrix}. \tag{4}$$

The optimal value of the factors might differ depending on the value of the uncertainties and the amount of each type of observation that is assimilated (Tian et al., 2017).

Observation space covariance localization

The covariance localization approach is typically used in the field of DA to mitigate the impact of spurious long-range correlations in model ensemble statistics, which can negatively affect the DA update, especially when small ensemble sizes are used (Houtekamer and Mitchell, 1998; Hamill et al., 2001). In short, the approach consists of damping correlations that are above a defined radius that represents the expected correlation range.

Previous studies by Zhao and Yang (2018); Khaki and Awange (2019); Girotto et al. (2019); Tangdamrongsub et al. (2022); Wongchuig et al. (2024) implement observation space covariance localization, where correlations between model variables and observations are damped based on the distance between them. This type of localization ensures that each model variable is influenced only by nearby observations that could realistically affect them (Fig. 2b).

The localization can be discrete (i.e., all observations further than a cutoff radius should be ignored, Houtekamer and Mitchell, 1998) or smooth (i.e., the observations are weighted depending on their distance to each model grid cell, Houtekamer and Mitchell, 2001). Domain localization or local analysis (Mitchell and Houtekamer, 2000; Evensen, 2003) can also be seen as a type of discrete observation space covariance localization. Smooth observation space localization matrices are typically built based on compactly supported distant-dependent functions, such as Gaspari-Cohn functions (Gaspari and Cohn, 1999). The localization matrix $(\rho_{1/2})$ is then applied to the predicted model-observation covariance matrix $(C(X_k^-)A^\top)$ through a Schur (elementwise) multiplication, resulting in the following Kalman gain (Houtekamer and Mitchell, 2001)

$$K_k = \rho_1 \circ (C(X_k^-)A^\top)(\rho_2 \circ (AC(X_k^-)A^\top) + \Sigma_{y^o,k})^{-1}. \tag{5}$$

https://doi.org/10.5194/egusphere-2025-5625
Preprint. Discussion started: 20 January 2026

The localization radius typically reflects the expected radius of influence of each observation, and thus larger localization radii are typically assigned to TWS observations ($3° - 10°$ in previous studies) and smaller radii to SSM observations ($0.25° - 3°$ in previous studies, Table 1, Fig. 2b). In this study, we call this "observation space mixed localization".

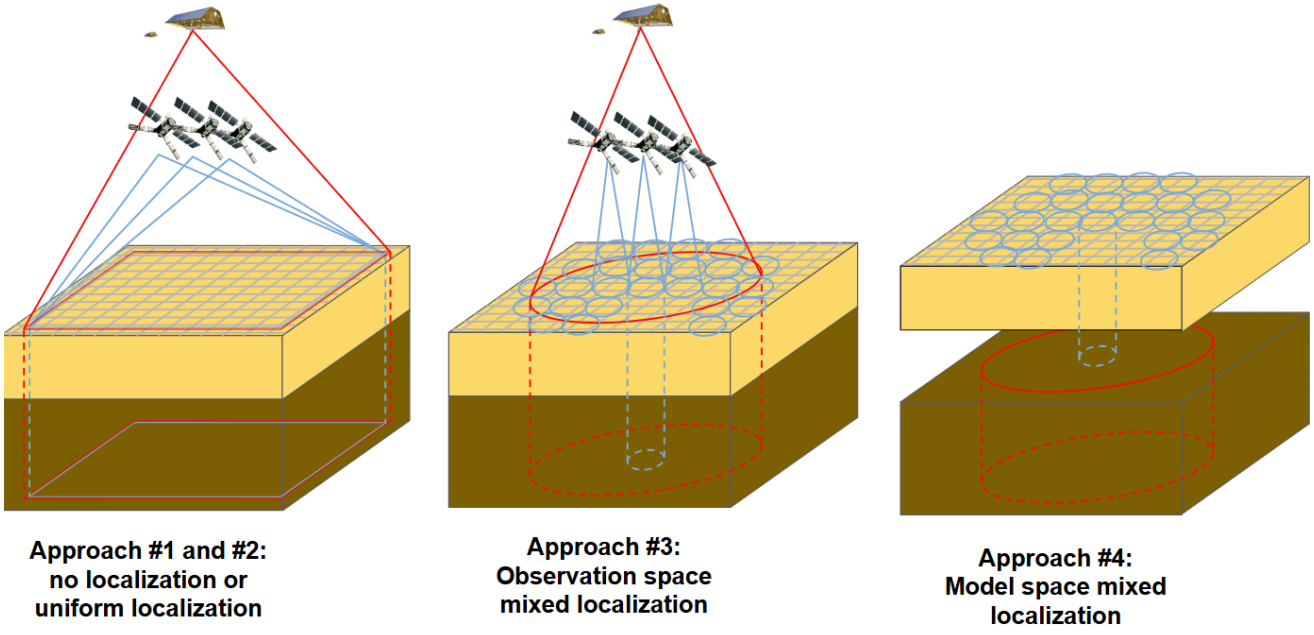

Figure 2. Diagram of different covariance localization approaches considered in this study. In the first two diagrams, the red and blue lines represent the area of influence of TWS and SSM observations, respectively. In the diagram on left (Approach #1 and #2), each SSM and TWS observations can influence a broad area, where spatial update distribution patterns will be constrained by ensemble statistics. In the middle diagram (Approach #3), the influence of SSM observations is concentrated on smaller regions (blue circles), while TWS observations update model estimates in a broader area (red circle) (Eq. 5). In the diagram on right (Approach #4), the blue cylinders represent the model space localization of SSM as well as SSM - groundwater correlations, and the red circle represents the broader model space localization of the groundwater (Eq. 6). The dark brown cube represents the groundwater component of the model, and the yellow cube represents the SSM component of the model.

Model space covariance localization

In addition to observation space covariance localization, it is also possible to implement a model space covariance localization (Campbell et al., 2010) (Fig. 2c). In this approach, localization is applied to the matrix $C(X_k^-)$, which represents the ensemble-based error correlation between the model state variables. In other words, correlations between model grid cells with other model grid cells are damped depending on their distance, no matter the kind of assimilated observation or location of the observations.

The localization is typically performed through smooth distant-dependent functions such as the Gaspari-Cohn function, and applied to the covariance matrix through a Schur multiplication, that is, $\rho \circ C(X_k^-)$ (Campbell et al., 2010), so that the Kalman

https://doi.org/10.5194/egusphere-2025-5625
Preprint. Discussion started: 20 January 2026

gain is expressed as

$$K_k = (\rho \circ C(X_k^-))A^\top (A(\rho \circ C(X_k^-))A^\top + \Sigma_{y^o,k})^{-1}. \quad (6)$$

Here, the localization radius should reflect the expected spatial variability of water storage. Although it is possible to define a unique localization radius for all water storage components (see, e.g., Retegui-Schiettekatte et al., 2025b, working with TWS DA), it might be more realistic to consider different localization radii for different vertical water storage compartments (e.g., a sharper localization might be applied to SSM compared to groundwater, Fig. 2c). This second approach is the one we propose in this study and is from now on called "model space mixed localization". In a previous work performing daily TWS DA, it was found that the groundwater localization half-radius should be larger than 3° to avoid too sharp groundwater storage updates during DA (Retegui-Schiettekatte et al., 2025a).

Model space covariance localization is especially useful when working with non-local observations (Campbell et al., 2010; Lei et al., 2018), where computing a distance between observations and model variables is not straightforward (e.g., when TWS is assimilated as a sub-basin average, it is not clear which is the "position" of the observation, and taking the geometrical center of the sub-basin as a reference might decrease the influence of the observations around the sub-basin edges). One of its main drawbacks is the need to explicitly calculate the matrix $C(X_k^-)$ (of dimension $\sim 34000 \times 34000$ in our experiment) and its Schur multiplication with the matrix ρ, of the same dimension, which can be very memory intensive (Campbell et al., 2010).

In this study, four different tuning approaches are compared: Approach #1 is a plain multi-variate DA without tuning; Approach #2 applies observation uncertainty adjustment; Approach #3 applies observation space mixed localization; and Approach #4 applies model space mixed localization (see more details of the implementations in Section 3.1). It is worth noting that the Approaches #3 and #4 do not include any observation uncertainty adjustment (Approach #2), and Approach #4 does not require any additional observation space localization such as that in the Approach #3.

2.3.4 Kalman Gain matrix and simplified representation

One of the interesting aspects of this work is the evaluation of the Kalman gain (K) structure in different DA settings (Section 4.2). In this section, we delve deeper into the meaning of the Kalman gain and the simplified view displayed in the manuscript.

K (or K_k, where k indicates a specific timestep) is the element in the EnKF equations that determines the extent to which each observation will impact each model variable (see the EnKF equations in Section 2.3.1). The structure of K exclusively depends on the model error structure and observation error structure (Eq. 2), and can be modified through DA tuning approaches such as observation uncertainty adjustment and localization (see Eqs. 4, 5 and 6). Note that the final impact of each observation on the model will also depend on the difference between observations and model predictions $(Y_k^o - AX_k^-)$, see Eq. 1, but for the sake of simplicity this factor is omitted from our investigations.

Each column of K corresponds to one observation (i.e., in this study, 3 columns for sub-basin averaged TWS observations, and up to 368 columns for SSM observations). Each row of K corresponds to one model variable (that is, a water storage compartment in a model grid cell, with 8 water storage compartments and 4226 model grid cells, resulting in $8 \times 4226 = 33.808$

https://doi.org/10.5194/egusphere-2025-5625
Preprint. Discussion started: 20 January 2026

model variables). The matrix element in the row i and column j represents the impact that the observation number j will have on the model variable number i.

Analyzing the structure of K allows us to investigate the impact of each observation on each of the model variables. However, K typically has very large dimensions (33.808×371 in this study), making it difficult to visualize and analyze. To ease this task, in Section 4.2 we represent a "simplified view" of K by selecting some representative observations and model variables. In this simplified view, columns 1-3 represent the three sub-basin averaged TWS observations, and columns 4-12 represent 9 selected SSM observations. Likewise, rows 1-3 represent the model sub-basin averaged TWS; rows 4-8 represent model SSM in grid cells for which SSM observations are available and rows 9-12 represent model SSM in grid cells for which no SSM observations are available. The value of each of the matrix elements is represented by a color scale, and the matrix is separated into blocks to facilitate its interpretation. Additional details on the computations of the simplified K displayed in the manuscript are available in Section 3.2.

3 Experimental setting

3.1 Model run and DA

Model run

The W3RA model was used to perform the experiments. The model run was carried out for the Ganges-Brahmaputra-Meghna river system area, in a daily and 10 km resolution, with forcing data derived from ERA5 and ERA5-Land (see Section 2.2). An ensemble of $N_e = 30$ model realizations was generated by perturbing the forcing fields and the parameters of the model according to their own uncertainties, following the approach of Renzullo et al. (2014). The model was warmed up for the period 2000-2003 to reach an appropriate ensemble spread in the water storage estimates. The run was extended from 2003 to 2015 to generate the Open Loop (OL) solution.

Observation pre-processing

An observation pre-processing was performed before DA. As the modeled and satellite-retrieved SSM typically refer to different soil depths, SSM observations were rescaled so that their statistics match those of the model via cdf-matching (Reichle and Koster, 2005), and the SSM uncertainties provided by ESA CCI were also rescaled accordingly. The ESA CCI tiles for which less than 50 % observations were available were excluded from the DA process (the remaining tiles are colored red in Fig. 1). In the case of TWS, the temporal mean of the sub-basin averaged TWS time series was adjusted to that of the model, but the time series were not rescaled to avoid modifying the amplitude of seasonal, inter-annual and decadal variability, which might be overestimated or underestimated within the model. Both observations were perturbed using a Cholesky decomposition approach and according to their respective uncertainties (koc, 2007; Schumacher, 2016).

The trends of GRACE TWS in the East and West sub-basins include, among others, ice water loss due to glacier retreat in the Himalayan mountains (Wouters et al., 2019; Sherpa and Werth, 2025), but W3RA does not model glaciers. Glacier retreat rates are available from previous work based on satellite stereo imagery (see Section 2.2), and therefore a possibility would be to exclude these glacier declines from TWS before DA. However, in this study, we do not apply this reduction to equate the

https://doi.org/10.5194/egusphere-2025-5625
Preprint. Discussion started: 20 January 2026

experimental conditions to regions where no robust glacier retreat estimates are available. As part of the evaluation, we assess how the W3RA accommodates these trends, and we deduct them from groundwater after the DA and before the validation.

Data Assimilation

All DA experiments were performed for the period September 2003 to December 2015, in the three sub-basins in Fig. 1. The DA update occurs at the end of each daily timestep following the method described in Sections 2.3.1 and 2.3.2. In addition to the multi-variate DA, uni-variate (i.e., single-observation) TWS DA and SSM DA experiments were also run for comparison.

The TWS observations were assimilated as a summation of all the W3RA land water storage components, including runoff water, topsoil, shallow soil, deep soil and groundwater (see Table 2), and as a sub-basin averaged field (Fig. 1). SSM was assimilated into the topsoil and shallow soil components, as an average over the $0.25° \times 0.25°$ ESA CCI tiles (Fig. 1). Although the ESA CCI SSM corresponds to the first few centimenters of the soil, and therefore could be equated to the model topsoil, due to the small field capacity of shallow soil we decided to update these two compartments jointly (in this manuscript the summation of both is referred to as SSM). The motivation behind this decision was to simplify the design of the mixed localization for the different localization implementations, as well as the evaluation of the results. Equating a deeper model soil layer with satellite-derived soil moisture could lead to a systematic phase difference between them, where satellite soil moisture variations precede model variations. However, this was not the case in this study, with satellite soil moisture peaking and decaying later in the season compared to model SSM estimates (Section 4.3.2). Note that, to further simplify localization and validation, deep soil water and groundwater are also treated jointly (the summation of both is here referred to as groundwater).

In all DA experiments, river water and snow compartments were excluded from the DA update step as it was found that including them led to degradations in these compartments (see Appendix D), and the vegetation water storage compartment was also excluded due to its marginal contribution to the variability of TWS in the basin. The water storage estimates of the river, snow and vegetation of the model were subtracted from the TWS observations prior to assimilation. As a result, 8 vertical water storage compartment variables were updated in the DA process, these being the gridded runoff water (1 variable), the topsoil, shallow soil and deep soil water estimated for two different hydrological units (6 variables) and groundwater (1 variable).

DA tuning approaches

The novel approach suggested and analyzed in this study (Approach #4) implements a model space mixed covariance localization. To the best of our knowledge, this is the first time such an approach has been implemented in a multi-variate land DA experiment. The localization was defined through a Gaspari-Cohn function (see Section 2.3.3). A localization half-radius of $0.5°$ (based on Girotto et al., 2019) was applied to SSM, as well as to the covariance between SSM and groundwater; and a half-radius of $10°$ was applied to groundwater. Although a smaller groundwater localization half-radius of $3°$ was initially deemed more appropriate (based on Retegui-Schiettekatte et al., 2025a), this was found to produce very sharp anomalies in groundwater estimates. Finally, a half-radius of $10°$ was adopted to enhance smoother groundwater variability patterns. In both cases, the values are in the range of TWS localization degrees reported in the literature (see Table 1).

For comparison, three other approaches were implemented based on the previous literature. Approach #1 was a plain multi-variate DA run without any tuning. In Approach #2, (uncertainty adjustment), SSM uncertainty multiplier factors of $\alpha_{SM} =$

https://doi.org/10.5194/egusphere-2025-5625
Preprint. Discussion started: 20 January 2026

$1, 2, 5, 10, 15, 30, 60, 240$ were considered, while α_{TWS} was kept to 1. Approach #3 (observation space mixed localization) was implemented by applying a smooth localization based on a Gaspari-Cohn function. For consistency with the model space localization, an influence half-radius of $10°$ was used for the TWS observations and $0.5°$ for the SSM observations.

3.2 Assessment of the DA performance

For the evaluation and validation stage, all model estimates were averaged over the 30-member ensemble. Standard metrics such as standard deviation (STD), root mean square difference (RMSD), Nash-Sutcliffe efficiency (NSE), Pearson correlation coefficient (here generically referred to as correlation coefficient) and its corresponding p-value were used. All validations were performed over the whole study period (2004-2015). A Theil-Sen trend estimate with a Mann-Kendall significance test was used to compute the declines in land water storage in Section 4.4.

Kalman gain

The Kalman gain here displayed was computed based on the model covariance structure of the 1st of July of 2004. This date was chosen because of the high correlation between SSM and TWS that appear on this date, which leads to notable cross-variable influences and therefore helps to explain the results observed in the DA experiments. Regarding the observation covariance structure, average errors of 3.31 mm and 13.38 mm were taken for all SSM and TWS observations, respectively.

Groundwater validation

The groundwater validation is performed on an inter-annual timescale, which is derived by averaging the time series on a sliding window of 12 months. This smoothing technique is consistent with the aggregation process included in the computation of SPEI-12 time series. The in situ groundwater time series presented many small gaps that, if left unaddressed, generated larger 12-month gaps after the smoothing process. Therefore, a gap-filling algorithm was applied before smoothing (see more details in Appendix A). For spatial validation of groundwater variability, a clustering based on Principal Component Analysis (PCA) was performed on the observed groundwater level time series (more details on PCA can be found in Forootan and Kusche, 2012; Retegui-Schiettekatte et al., 2025b). Groundwater sites for which the first principal component contributed to more than 65 % of the variability were included in cluster 1, and all other sites were included in cluster 2. Groundwater validation was only performed in terms of correlation coefficients due to the inherent scale difference between groundwater storage, groundwater level, and SPEI estimates.

TWS time series in the region are affected by declines caused by glacier retreat which, when assimilated into the model, are allocated to the groundwater component. Before any groundwater comparison, this decline was deducted from the groundwater time series. Hugonnet et al. (2021) suggest that glacier retreat does not show strong inter-annual changes between 2004 and 2016 in this region, and therefore we approximated the impact as a linear trend. The impact of this retreat on the sub-basin averaged TWS was calculated as $\Delta S_{subb} = \Delta S_{glac} \cdot \frac{A_{glac}}{A_{subb}}$, where A_{subb} and A_{glac} are the area of each sub-basin and of the glaciers of each sub-basin, respectively, and ΔS_{glac} is the equivalent decrease in water storage produced by the glacier retreat and was derived from previous studies (see Section 2.2).

River water level validation

https://doi.org/10.5194/egusphere-2025-5625
Preprint. Discussion started: 20 January 2026

The river water storage validation was performed against in situ water level time series. As these two variables are related through the cross-section of the river, which is here unknown, the model estimates were rescaled to match the observation in mean and STD before computing the Nash-Sutcliffe efficiency.

4 Results and Discussion

4.1 Evaluation against assimilated data

In this section, we assess the skill of the new approach proposed in this study, the model space mixed localization (Approach #4). The evaluation is based on the RMSD relative to the assimilated datasets (i.e., ESA CCI SSM and GRACE TWS) and is therefore intended only to verify whether the satellite-derived dynamics were correctly transferred to the target model variables. In addition, we qualitatively evaluate the performance of the assimilation technique in disaggregating its updates into individual storage components based on the model ensemble statistics.

Starting with the uni-variate experiments, evaluating the DA results against the assimilated observations indicates that the observed SSM and TWS dynamics were successfully transferred into the model (Table C1, Fig. 3a-h). The uni-variate SSM DA reduces the RMSD of the modeled and observed SSM from 13.6 mm to 3.8 mm on average in all 0.25° tiles in which the DA was performed (Fig. 3b). The SSM is found to be predominantly modified during the unsaturated period, changing the timing of the recharge period (April-May) and its decay period (October-March) (Fig. 3a, see also a zoom in a shorter period in Fig. B1 of Appendix B). The uni-variate TWS DA leads to TWS RMSDs below 7 mm for the three sub-basins with respect to GRACE, reflecting a notable improvement with respect to OL TWS which has initial discrepancies of 80 - 113 mm in terms of RMSD (Fig. 3h). Note that river, snow, and vegetation water storage were excluded from the assessment as these components were not modified in the DA process. The TWS estimates are modified in the seasonal to inter-annual timescale (Fig. 3e), as well as in the sub-seasonal timescale (for example, see June and September 2004 in Fig. B1 of the Appendix B).

Comparing the uni-variate TWS results with SSM observations and vice versa can be considered as an independent validation, as only one kind of observation was involved in each uni-variate experiment. The uni-variate TWS DA has a small impact on the SSM estimates (average degradation with respect to OL is less than 10 % of the RMSD value, see Fig. 3d), and the uni-variate SSM DA also shows a very light impact on the TWS estimates (RMSD modified by less than 10 %, see Fig. 3f).

By applying the multi-variate DA, improvements similar to the uni-variate experiments are reached for both SSM and TWS variables, with only minimal differences (RMSD reduced to below 10 mm for sub-basin averaged TWS and an average of 3.8 mm for the 0.25° tile SSM; see Figs. 3c and 3g). This shows that the setting of the multi-variate DA has correctly constrained the SSM and the summation of all the vertical components.

A successful modification of horizontally and vertically aggregated variables (e.g. sub-basin averaged TWS or tile-averaged SSM) does not guaranty a realistic update of the underlying distributed estimates ($0.1° \times 0.1°$ grid) and individual water storage compartments (Retegui-Schiettekatte et al., 2025a, b). In Fig. 4, the impact of the DA experiments in disaggregated model estimates is represented (in terms of STD with respect to OL estimates).

https://doi.org/10.5194/egusphere-2025-5625
Preprint. Discussion started: 20 January 2026

	RMSD (mm)			
	OL	DA		
		SSM	Multi-v.	TWS
TWS East	112.8	111.5	6.4	5.2
TWS West	147.6	145.3	9.5	7.0
TWS South	80.6	84.1	6.4	3.1
SSM average	13.6	3.8	3.8	14.3
SSM min	4.9	1.2	1.2	4.9
SSM max	24.9	8.7	8.7	25.3

Table 3. RMSD of model estimates (OL, SSM DA, multi-variate DA and TWS DA) with respect to assimilated data. SSM min and SSM max refer to the minimum and maximum RMSD values across the $0.25° \times 0.25°$ tiles.

Regarding SSM, all DA experiments result in a smooth spatial distribution of updates (Fig. 4e-h). It should be noted that regions in which SSM observation was not assimilated (e.g., Himalayan Mountains) are also updated in the multi-variate and TWS DA process (more details in Section 4.2).

The negative trends introduced in groundwater show sharp spatial patterns (Fig. 4j-k), leading to notably high RMSD values (up to 3000 mm in some areas of the Himalayan mountains, for multi-variate DA). Different patterns arise in the uni-variate TWS DA and the multi-variate DA; in the latter, areas where SSM is assimilated display smoother groundwater patterns, and sharp patterns are constrained to areas where no SSM was assimilated. This could suggest that constraining soil moisture fields through SSM observations helps regulate the spatial distribution of updates in groundwater. Note that groundwater is the only land water storage compartment that exhibits negative trends, and therefore these must include the trends induced by glacier decline (see more details in Section 4.3.1).

The disaggregation reveals that the uni-variate TWS DA and the multi-variate DA introduce a negative trend to the river water storage estimates (Fig. 4b-d). As the river water compartment was not included in the DA process, this trend can be fully attributed to decreasing groundwater values, which has a direct impact on streamflow through baseflow generation.

https://doi.org/10.5194/egusphere-2025-5625
Preprint. Discussion started: 20 January 2026

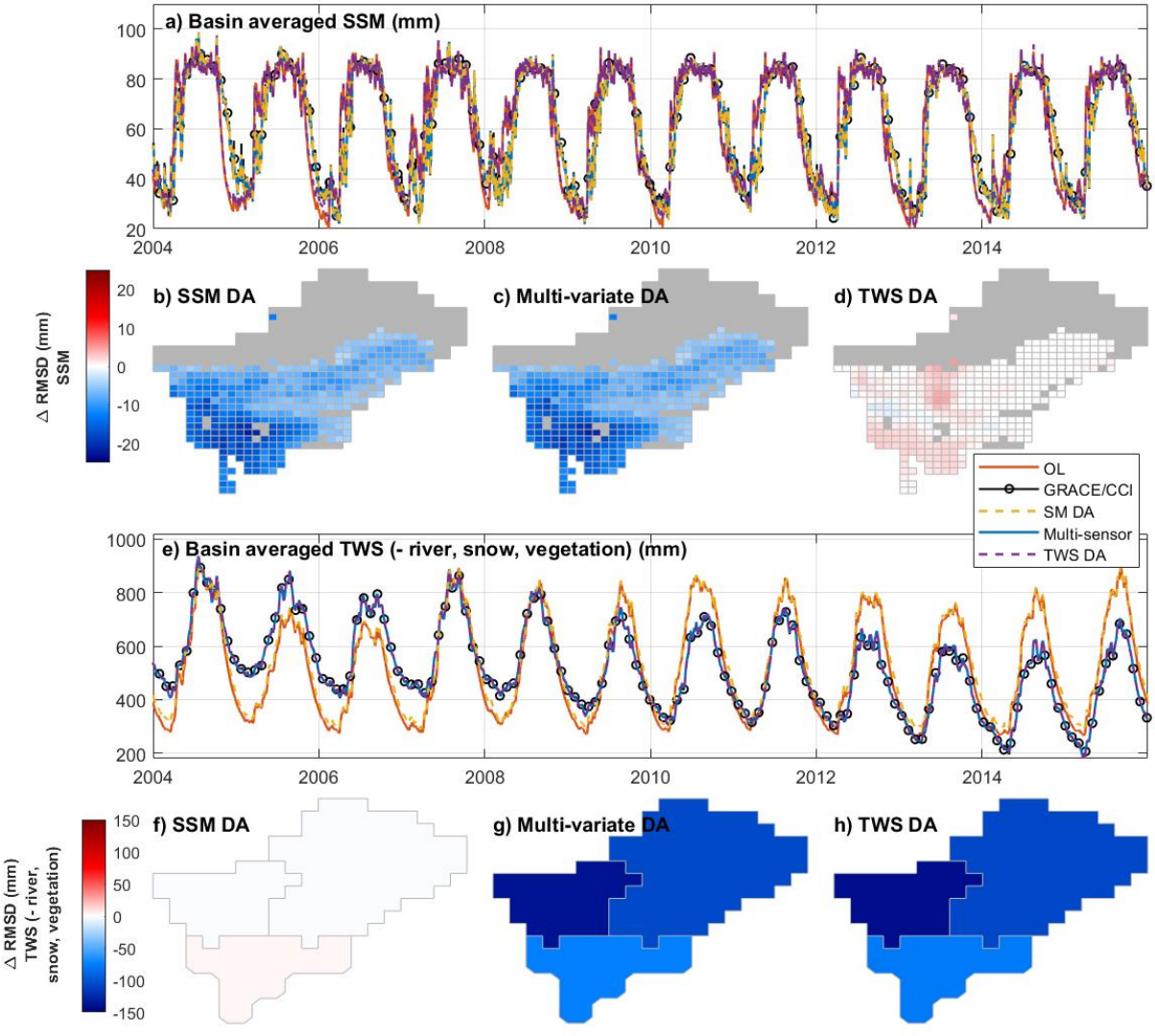

Figure 3. Basin averaged time series of SSM and TWS (a,e) and improvement in the RMSD of tile-averaged SSM (b-d) and sub-basin averaged TWS (f-h) of the model, after different DA experiments. ΔRMSD is defined as the RSMD of the DA product minus the RMSD of the OL, where the RMSD is computed by taking the assimilated data as a reference. (b, d) show the impact of the uni-variate SSM DA, (c, g) show the impact of multi-variate SSM and TWS DA and (d, h) shows the impact of the uni-variate TWS DA. For (b-d), ESA CCI tiles where no observation was assimilated have been shaded (gray area).

https://doi.org/10.5194/egusphere-2025-5625
Preprint. Discussion started: 20 January 2026

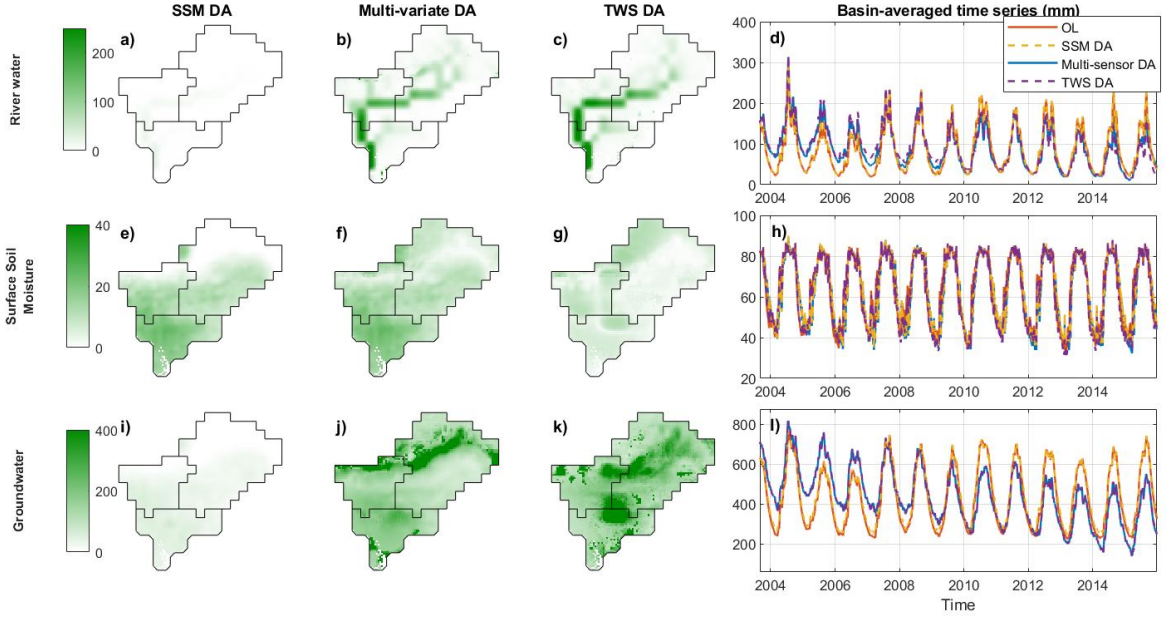

Figure 4. Standard deviation of DA minus OL on spatially distributed ($0.1^\circ \times 0.1^\circ$ grid) model estimates for river water (a-c), SSM (e-g) and groundwater (i-k). The standard deviation is expressed in mm. The column in the right (d, h, l) shows basin-averaged time series for the same variables.

https://doi.org/10.5194/egusphere-2025-5625
Preprint. Discussion started: 20 January 2026

4.2 Comparing different DA approaches

This section compares the Approach #4 with the results obtained by using other multi-variate DA approaches suggested in the previous literature (Approaches #1-#3). The objective of this comparison is to understand the impact of the different approaches on the DA process and to study the benefits of Approach #4 proposed in this study (see Section 2.3.3 for more details of the approaches). In this paper, the descriptions are mostly qualitative, but numerical values can be found in Appendix C.

Approach #1 consists of a plain (non-localized and non-adjusted) multi-variate DA. The evaluation shows notable improvements in the SSM component (Fig. 5a), but limited improvements in the TWS estimates (Fig. 5e). In the TWS time series it can be observed that strong peaks caused by SSM updates reduce the agreement between modeled and observed TWS (Fig. C1 of Appendix C). A similar effect was reported by Tian et al. (2017) where the SSM observations were found to dominate over the TWS observations. They attributed the effect to two factors: (i) the lower uncertainty of the SSM observations (e.g., 3.31 mm on average in our study) compared to the TWS observations (e.g., 13.38 mm on average in our study); and (ii) the higher number of SSM observations (up to 368 per day in this study, due to the $0.25°$ resolution) compared to the TWS observations (3 sub-basin averaged values per day). Note that Zhao and Yang (2018) reported the opposite effect, with TWS dominating the SSM modifications. In that case, TWS was assimilated at daily, $1° \times 1°$ resolution, and the brightness temperature was assimilated at daily, $0.9° \times 1.25°$ resolution, that is, both with a similar spatial-temporal sampling. A stationary error of 2K was used for the brightness temperature and a spatially variable error of unspecified magnitude for TWS. It is therefore possible that, under similar sampling conditions, a too low error for TWS might have favored these observations over the brightness temperature, which would be consistent with the explanation of Tian et al. (2017).

This effect is very well reflected in the structure of the Kalman gain matrix (K) for the 1st of July 2004. Fig. 5i shows a simplified representation of K (see more details on the meaning of K and the simplified representation in Section 2.3.4). The impact of the observations on model sub-basin averaged TWS is represented by the intensity of the colors in the upper blocks. We see that SSM observations have an impact that is similar in intensity to TWS observations (upper right and upper left blocks, respectively), reflecting the high influence of SSM observations on modeled TWS.

Approach #2. To remedy this issue, Tian et al. (2017) suggested increasing the uncertainty of the SSM observations and reducing that of the TWS observations, to enhance the impact of TWS observations. One of the challenges of this approach is that the appropriate adjustment factor must be found heuristically. In our case, a multiplying factor of $\alpha_{SSM} = 10$ was found to lead to notable improvements in TWS, but reduce the improvement in SSM (Fig. 5b and f; higher factors lead to degradations in SSM). A similar effect was also reported by Tian et al. (2017) explaining that adjusting the uncertainty allows us to reach a compromise between improvements in TWS and SSM, but might not lead to optimal results for these two variables compared to uni-variate DA. The effect was attributed to conflicting constraints introduced by the TWS and SSM observations, which could end up canceling each other. In contrast, Khaki and Awange (2019); Khaki et al. (2019, 2020) report an improved performance of multi-variate DA with respect to uni-variate DA, suggesting that in that study case the constraints introduced by TWS and SSM DA in their study region might enhance each other instead of canceling each other.

https://doi.org/10.5194/egusphere-2025-5625
Preprint. Discussion started: 20 January 2026

The structure of K in this approach shows that the impact of SSM observations on model TWS estimates is considerably reduced compared to approach #1 (upper right part, Fig. 5j, has lighter colors) but so is their impact on model SSM (central right part). This confirms that the uncertainty adjustment approach offers a compromise between improvements in SSM and TWS, but can be limited due to a significant cross-influence of TWS observations on model SSM and vice versa.

Approach #1 and #2 also display a generally limited improvement in terms of SSM when compared to Approach #3 and #4, even in uni-variate SSM DA experiments (not shown here), due to the strong basin-wide constraints introduced by non-localized model statistics, which makes it difficult to improve SSM estimates locally. This issue is better handled using localized DA (Approaches #3 and #4).

The **approach #3** consists in implementing a mixed observation space covariance localization, similar to that presented by Girotto et al. (2019); Tangdamrongsub et al. (2020) and Wongchuig et al. (2024) (this approach does not include any observation uncertainty adjustment like in Approach #2). The approach is found to lead to notable improvements in both the SSM and the TWS estimates (Fig. 5c and g).

Looking at the matrix K provides insight to explain these results (Fig. 5k). First, the localization approach allows to concentrate the impact of each SSM satellite observation in a local region instead of the whole basin (see Fig. 2). This means that each SSM observation can strongly update model estimates in their region of influence, therefore, better modifying the SSM compared to Approaches #1 and #2. Additionally, it means that each SSM observation will have a limited impact at the basin scale (central right block of K in Fig. 5k). As a consequence, the impact of SSM on the sub-basin averaged TWS is kept low without the need of an uncertainty adjustment (upper right block). Second, the impact of TWS observations on SSM estimates is very low for regions where SSM observations are available (left central block), likely because these SSM estimates are already strongly constrained by the SSM observations. These facts support two conclusions: (i) localization approaches can be used to regulate the relative impact of different observations in a multi-variate DA framework; and (ii) localization can reduce the cross-influence of TWS observations on SSM and vice versa. Note that the key to these two achievements lies in mixed localization, that is, applying different localization degrees for TWS and SSM observations; studies that implement a uniform localization do not report the same results (e.g., Zhao and Yang, 2018)

Despite these benefits, one notable drawback for this approach was found: TWS observations here have a strong impact on model SSM estimates in areas where no SSM observations are available, such as the Himalayan Mountains (Fig. 5m and the lower left block of K in Fig. 5k). In our experiment, this results in a general negative SSM trend for the entire basin, which is likely unrealistic (Fig. 5o). This aspect could explain why our results contrast with those reported by Girotto et al. (2019); Tangdamrongsub et al. (2020); Wongchuig et al. (2024). These studies report a reduced effectiveness of multi-variate DA compared to uni-variate approaches. A likely reason could be the sequential or asynchronous assimilation of TWS and SSM observations in their approaches, meaning that the TWS and SSM observations are not (always) assimilated simultaneously. The fact that either TWS or SSM is unconstrained during the DA update could have enhanced the cross-influence between them, leading to problems when the observations introduce conflicting or anti-correlated updates. Although this explanation is plausible, further investigation is needed to confirm it and better understand how the cross-variable influence works in asynchronous DA.

https://doi.org/10.5194/egusphere-2025-5625
Preprint. Discussion started: 20 January 2026

Finally, **Approach #4** (model space mixed localization) displays similar benefits as Approach #3 (Fig. 5d and h) and additionally mitigates the impact of TWS observations on SSM in areas where no SSM observations are available (Figs. 5n), effectively preventing spurious trends in the SSM component (Figs. 5p). The key here is that localization is performed on the model space instead of the observation space (see Fig. 2), allowing to localize the impact of observations on SSM over the whole basin, regardless of the availability of SSM observations. In the K matrix (Fig. 5l), this can be seen in the left bottom block, showing a less intense impact of TWS on unobserved SSM estimates compared to Approach #3.

In summary, among the four strategies tested, Approach #4 is found to be the only one capable of completely reducing the influence of TWS on SSM and vice versa, thus marking a first in the resolution of cross-variable interference reported in previous studies. It is worth mentioning that model space localization is particularly suited for the integration of sub-basin averaged (i.e., non-local) observations, where defining an observation space localization can be challenging (Campbell et al., 2010). This approach was also found to avoid cross-variable influences in uni-variate TWS DA (see Section 4.1). The main limitation of this approach lies in the computational demand, as it requires the computation of the full model covariance matrix and a Schur operation in the model domain (Houtekamer and Mitchell, 1998; Campbell et al., 2010). This highlights the need for optimized implementations.

https://doi.org/10.5194/egusphere-2025-5625
Preprint. Discussion started: 20 January 2026

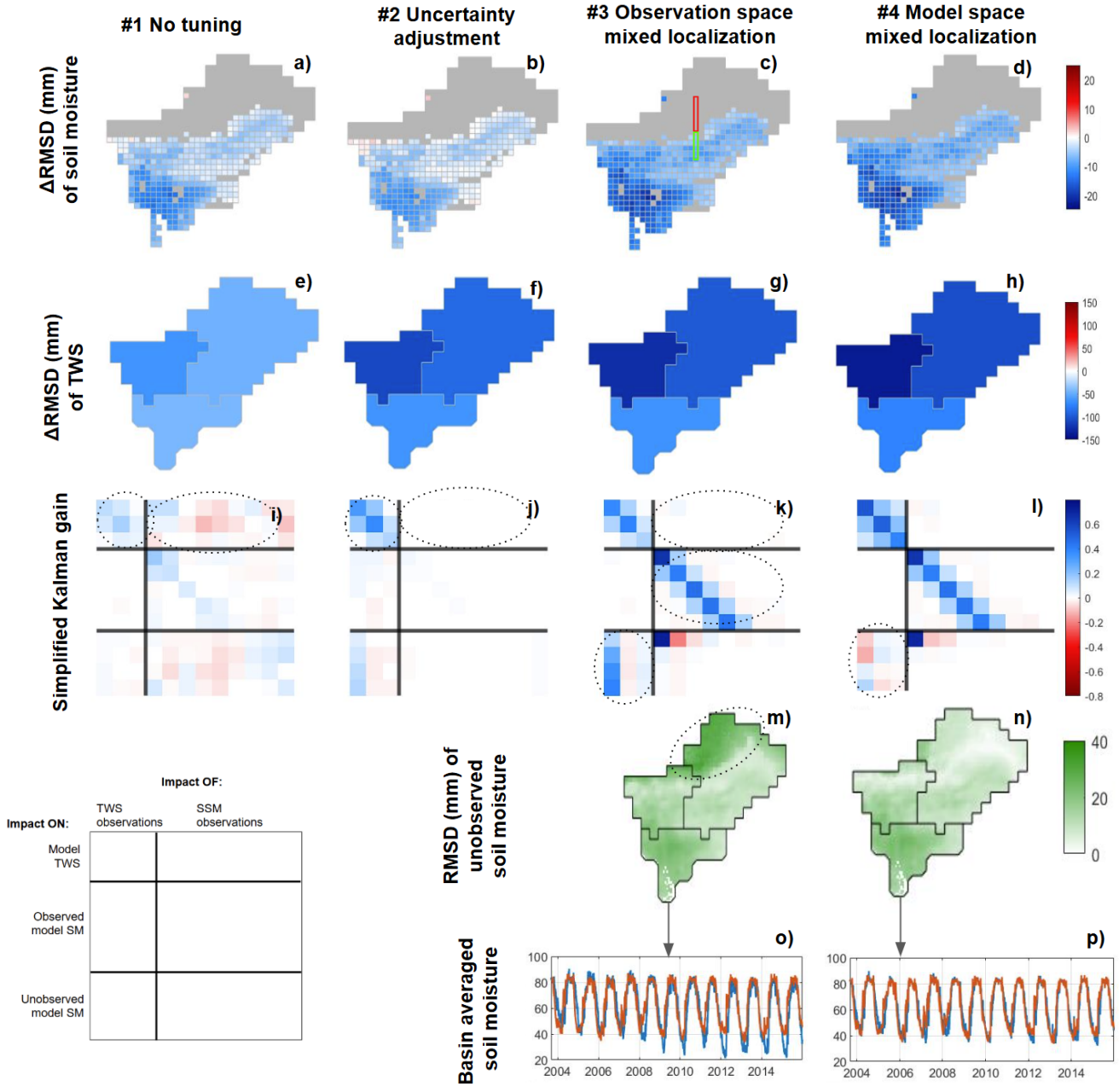

Figure 5. Result evaluation (a-h) and simplified K matrix (i-l) for multi-variate DA with different localization and uncertainty adjustment approaches. The result evaluation includes evaluation of modeled SSM against ESA CCI (a-d), evaluation of sub-basin averaged TWS against GRACE TWS (e-h) and evaluation of unobserved model SSM estimates (m, n), as well as comparison of sub-basin averaged SSM time series of OL (red) and multi-variate DA (blue) (o, p). A guide to interpret the simplified K matrix is provided in the lower left corner (see Section 2.3.4 for more details). In a-d, the gray area represents regions where no SSM observation was assimilated due to major gaps in the observations (i.e., Himalayan mountains). The red and green box in (c) show the observed and unobserved model SSM grid cells for which the simplified K is shown.

https://doi.org/10.5194/egusphere-2025-5625
Preprint. Discussion started: 20 January 2026

4.3 Evaluation against independent data

So far, we evaluated whether satellite-derived TWS and SSM dynamics were successfully transferred to the target model variables. In this section, we compare the DA results with independent data to test if the assimilation of TWS and SSM succeeds in bringing the model closer to reality. In light of the assessment of Section 4.2, we expect Approach #4 (model space mixed localization) to lead to the best results and therefore here we only present the validation of the multi-variate DA using Approach #4.

4.3.1 Groundwater

We first compare the sub-basin averaged DA results with the SPEI-12 index, which reflects hydrological wetness and dryness based on precipitation and evapotranspiration data. SPEI-12 is aggregated over a 12-month window, and therefore we apply the same treatment to the groundwater time series (Section 3.2).

The trends of GRACE TWS in the East and West sub-basins include, among others, ice water loss due to glacier retreat in the Himalayan mountains (Wouters et al., 2019; Sherpa and Werth, 2025), but W3RA does not model glaciers. In this study, we assimilated the whole TWS signal to see how the model accommodates these negative trends, and it was found that the trends were assimilated into the groundwater. As a consequence, before validating the inter-annual groundwater variability, we need to exclude glacier declines. As a conservative approach, the largest of the reported glacier trends are taken for this study (-0.63 m and -0.55 m of water equivalent per year, for the East and West sub-basin, respectively; see Table E1 of Appendix E). Validation using less conservative trends is also provided in Appendix E. The impact of glacier retreat on sub-basin averaged TWS is calculated following the method described in Section 3.2, and results in trends of -19.19 mm per year and -17.89 mm per year in the East and West sub-basins, respectively. After this reduction, groundwater shows a less pronounced negative trend that can be mainly attributed to land water variability. It should be noted that the South sub-basin has no glaciers and therefore does not require this treatment.

Although SPEI is standardized and is not suitable for validating the magnitude of groundwater variability, it reveals clear negative trends for the three sub-basins in the period 2004-2014 (Fig. 6). These trends, absent in the OL simulations, emerge distinctly through the multi-variate DA. Regarding the sub-decadal variability, multi-variate DA preserves the inter-annual variability of OL, but smooths certain anomalies (e.g., 2007 and 2010), possibly due to GRACE TWS resolution or interference with the decadal trends. In general, the correlation with SPEI improves significantly, from 0.15/0.24/0.57 (OL) to 0.60/0.78/0.81 (DA) for the East, West, and South sub-basins, respectively.

Monthly in situ groundwater levels (Shamsudduha et al., 2012, 2022), which are available for the area of Bangladesh, allow additional validation for the South sub-basin. Groundwater levels are related to groundwater storage through the specific yield, here unknown, so we perform the validation in terms of correlation coefficient. A validation of the groundwater estimates including seasonality does not show any notable improvement of DA (0.876 in correlation coefficient for OL and 0.884 for multi-variate DA), because the time series are dominated by the seasonal signal which mainly changes in amplitude (Fig. E2 of Appendix E). For this reason, we also applied the 12-month aggregation treatment to these time series to validate

https://doi.org/10.5194/egusphere-2025-5625
Preprint. Discussion started: 20 January 2026

the inter-annual variability and trend of the groundwater. Multi-variate DA markedly enhances groundwater estimates (Fig. 6c), increasing the correlation with groundwater levels from 0.49 (OL) to 0.73 (DA). A decadal trend is introduced, with higher groundwater levels in 2005–2008 than in 2013–2014. DA also displays realistic sub-decadal variability, capturing key anomalies such as the 2007 peak and the wet period of 2010–2011, which remain distinguishable despite the overarching negative trend.

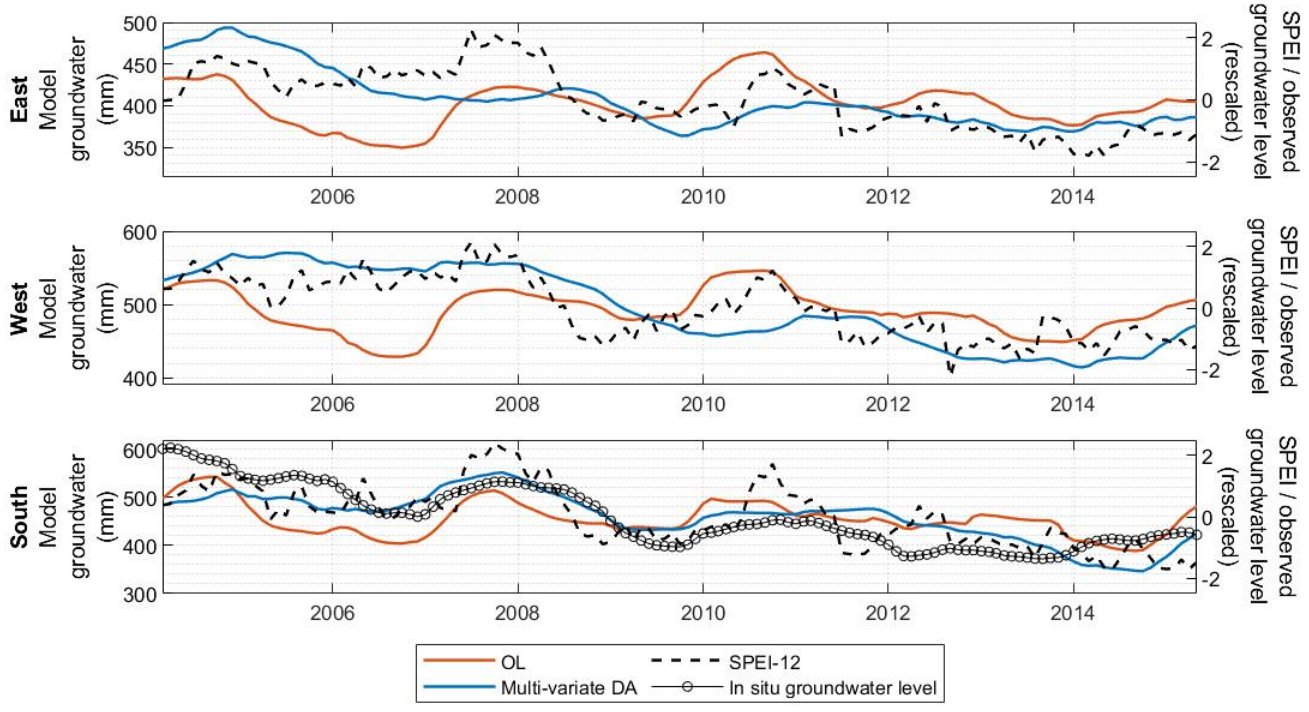

Figure 6. Inter-annual groundwater variability of OL and multi-variate DA; SPEI time series and groundwater level observations (rescaled, on the right axis).

	OL	Multi-variate DA
East sub-basin (ref. SPEI)	0.15	0.60
West sub-basin (ref. SPEI)	0.24	0.78
South sub-basin (ref. SPEI)	0.57	0.81
South sub-basin (ref. in situ)	0.49	0.73

Table 4. Correlation coefficient between modeled and independent groundwater storage variability estimation. All correlations are significant with p-value < 0.01.

https://doi.org/10.5194/egusphere-2025-5625
Preprint. Discussion started: 20 January 2026

Spatially distributed in situ groundwater level measurements allow us to validate the spatial groundwater patterns represented within the model for the South sub-basin. The results show a heterogeneous impact in different areas of the sub-basin (Fig. 7). To better interpret the results, a PCA-based clustering of in situ data is applied (see details in Section 3.2). For the sites belonging to the main cluster (Figs. 7 a, b, and c), overall improvements are observed as a consequence of the negative trends introduced by the multi-variate DA process, increasing the average correlation coefficient from 0.47 (OL) to 0.54 (multi-variate DA).

Notable degradations can be observed after DA for the remaining sites (Figs. 7 d and e), of which most are located close to the main rivers branches. The observed groundwater level of this cluster is characterized by a less strong trend, which might be explained by the fact that the presence of large river branches in these regions allows greater groundwater recharge, either through natural percolation processes or enhanced by anthropogenic actions (Shamsudduha et al., 2022). W3RA does not account for the feedback from the surface to the sub-surface components and therefore the DA is not informed about this mechanism. Thus, the inclusion of a negative trend in these regions reduces the average correlation from 0.33 (OL) to 0.28 (multi-variate DA).

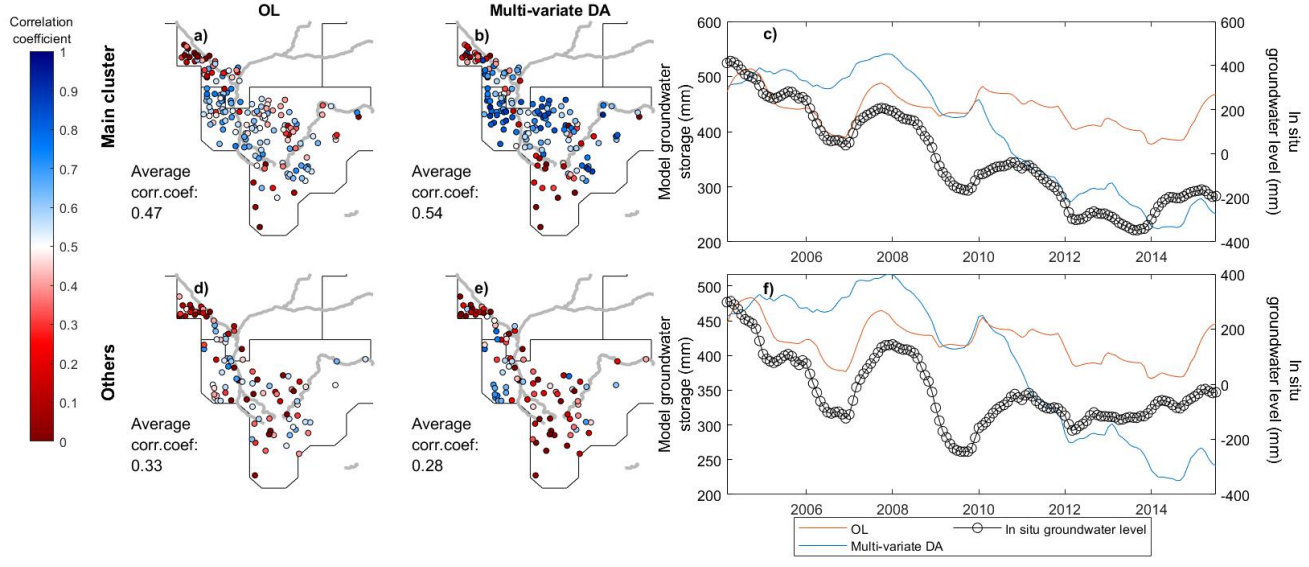

Figure 7. (a,b,d,e) Correlation coefficient between modeled groundwater storage and observed groundwater level for individual sites. The centerline of the main rivers of the region are added in the background as a reference. (c, f) Average groundwater storage and groundwater level time series for sites belonging to the main cluster (c) and remaining sites (f).

4.3.2 Surface soil moisture

Here we compare the OL and DA outputs with the soil simulations of the WaterGAP global hydrology and water use model (Döll et al., 2003; Müller Schmied et al., 2024; Nyenah et al., 2025). Although model outputs might be affected by limitations

https://doi.org/10.5194/egusphere-2025-5625
Preprint. Discussion started: 20 January 2026

such as errors in forcing data, process simplification, or missing representation of certain processes, they can provide an additional perspective to assess the realism of the DA results. The basin averaged time series show that, after multi-variate DA, SSM becomes saturated later in the season, and the decay of water at the end of the monsoon season is also slower (Fig. 8a). In other words, DA results mainly in a light phase shift in the SSM time series. The phase shift brings the estimates closer to those of the WaterGAP estimates.

The spatial distribution of the correlation between W3RA (OL) and WaterGAP is heterogeneous, with especially high discrepancies in areas with a sharp topography (slope >1 %, correlation coefficients mostly between 0.4-0.7, see triangles in Fig. 8b). There could be various reasons why the two models disagree in mountainous areas. First, the W3RA parameters are calibrated in Australia (a region without a high-mountain landscape) and later extrapolated to the world based on climatological and land use maps (van Dijk et al., 2013), while the WaterGAP parameters are calibrated against the outlet discharge of the East and West sub-basin in the Brahmaputra River basin (Müller Schmied et al., 2021) and, therefore, could have a more accurate representation of the soil water balance in the region. Second, snow melt, which is one of the input fluxes to SSM in mountainous areas, is also calculated differently in both models: although both use a degree-day approach, WaterGAP adapts the degree-day factor to a wide range of land covers, including ice, snow and bare land, while W3RA only accounts for tall and short vegetation covers (van Dijk et al., 2013; Müller Schmied et al., 2021). Taking this into account, it can be expected that WaterGAP is better adapted to the high-mountain environment of the Brahmaputra River basin.

The observed differences could also be related to the depth considered for the SSM components of W3RA and WaterGAP. The WaterGAP model only defines one soil moisture component, which is likely to reach deeper than the W3RA SSM. To exclude this possible cause, we have repeated a comparison equating WaterGAP SSM with the summation of all soil water storage components of W3RA (that is, topsoil, shallow soil, and deep soil, see Table 2). The results, reported in Appendix F, lead to conclusions similar to those presented here, thus excluding the depth difference as the origin of the disagreement.

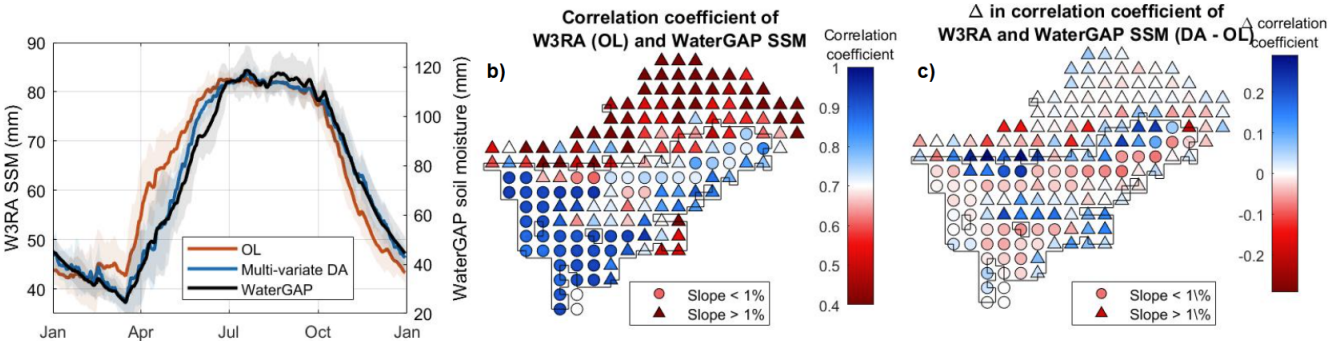

Figure 8. (a) SSM seasonality of W3RA OL, multi-variate DA and WaterGAP. (b) Distributed map of correlation coefficient of W3RA (OL) and WaterGAP, shown for the WaterGAP $0.5° \times 0.5°$ tiles. (c) Distributed map of change in correlation coefficient between W3RA and WaterGAP after DA. The black outline in (b) and (c) indicates the area where SSM observations were assimilated.

https://doi.org/10.5194/egusphere-2025-5625
Preprint. Discussion started: 20 January 2026

After DA, notable increases in the correlation with WaterGAP arise in these mountain regions, reaching increases of up to +0.3 correlation points in areas where SSM observations are available (Fig. 8c). Assuming that WaterGAP is better adapted to represent high-mountain hydrological processes, the results could indicate that the assimilation of ESA CCI SSM helps to better account for the impact of complex topography or snowmelt in SSM. However, these results should be interpreted with caution, as the WaterGAP model might also be affected by its own limitations in other aspects.

In the more flat regions located along the Brahmaputra River (slope <1 %, circles in Figs. 8b and c), for which the W3RA OL and WaterGAP estimates are more similar (correlation coefficients between 0.7-1.0), DA is found to slightly reduce the agreement between the two models by up to 0.1 correlation points. For the Himalayan Mountain area, where no SSM observation was assimilated, the impact of DA is driven by the TWS observations and leads to slight improvements and degradations.

4.3.3 River water

River water storage estimates are validated against in-situ river water level observations. We select the two sites that are closest to the outlet of the West and South sub-basins (water level data is not available for the East sub-basin, see site locations in Fig. 1). The OL time series show dynamics similar to the observed water levels (Fig. 9), with a high Nash-Sutcliffe efficiency (NSE) of 0.84 and 0.83 for the West and South sub-basins, respectively. The multi-variate DA introduces a decadal negative trend and inter-annual variability in both sub-basins, as can be noted by the higher river water storage values in 2004-2005 and notably lower values after 2010. As a consequence, the NSE is reduced to 0.75 and 0.74 for the West and South sub-basin, respectively, after DA.

Although river water storage was not directly updated during our DA experiments, the observed changes in discharge likely stem from trends and inter-annual variability introduced in groundwater by multi-variate DA, which then have an impact in streamflow through baseflow generation. Re-visiting runoff parameterization or applying joint Calibration/Data Assimilation (CDA; Eicker et al., 2014; Schumacher et al., 2018) could help refine this process. In addition, groundwater also includes negative trends related to glacier retreat (see Section4.3.1), which likely increases negative trends in river discharge. Incorporating a glacier component into the model representation and guaranteeing an accurate TWS trend partitioning between glacier and groundwater could help mitigate this issue.

Validation using detrended time series yields NSE values of 0.84/0.84 (OL) and 0.86/0.82 (DA) for the West and South sub-basins, respectively, suggesting that multi-sensor DA has limited influence on sub-annual discharge dynamics. This aligns with the findings of Ahmad et al. (2024), where SMAP SSM assimilation into Noah-MP showed minimal impact on streamflow in high-flow tributaries such as the Brahmaputra River. The broader literature also points to methodological choices, catchment characteristics, and land–river coupling limitations as key factors that restrict the impact of DA on river discharge (Massari et al., 2015; Brocca et al., 2017).

It is worth mentioning that we also attempted a multi-variate DA experiment in which we updated the river water storage compartment together with the land water storage states. The results are reported in detail in Appendix D, which show significant degradations in the sub-seasonal timescale. This suggests that to improve the surface water component in the Brahmaputra

https://doi.org/10.5194/egusphere-2025-5625
Preprint. Discussion started: 20 January 2026

River basin, a direct DA of water level measurements, such as lake and river altimetry, might be more beneficial than a SSM and TWS DA (see, e.g., Wongchuig et al., 2024).

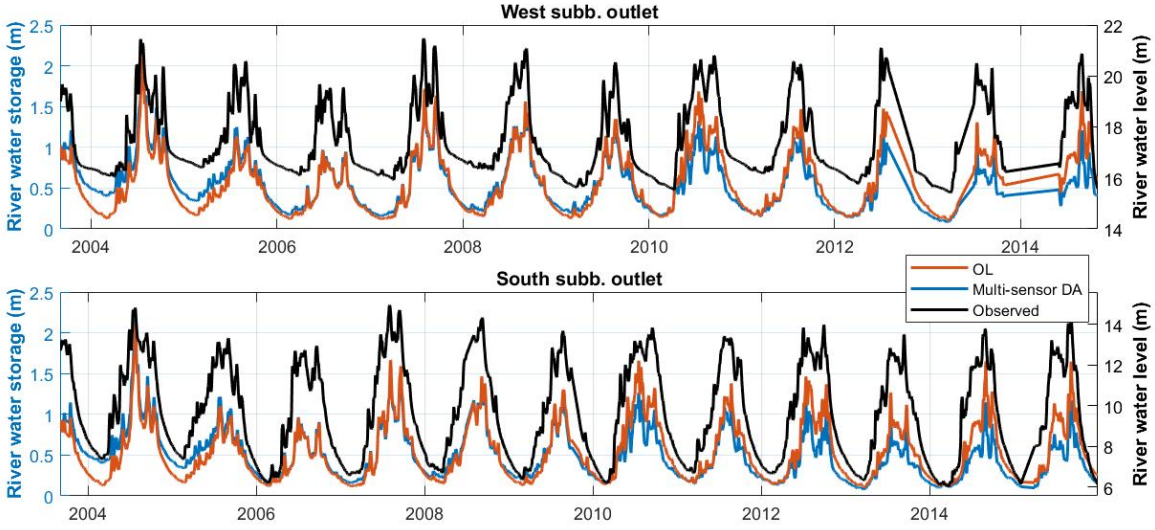

Figure 9. River water storage time series derived from OL (red) and multi-variate DA (blue), as well as in situ water level observations (black, with y axis on the right). The time series correspond to the two sites shown in Fig. 1.

4.4 Land water storage variability in Brahmaputra River Basin

The DA outputs show a higher realism than the initial model estimates (as shown in Section 4.3) while keeping the spatial and temporal resolution and continuity of the model. This leads to improved land water storage estimates that can be used to better monitor and understand the land hydrological variability of the Brahmaputra River basin. Here we perform a characterization of land water variability for the basin.

The basin averaged land (+ river) water storage time series is shown in Fig. 10. The middle line shows the inter-annual variability, which displays similar temporal patterns to those found for groundwater in Section 4.3.1. A Theil-Sen trend estimate reveals a significant decrease in land water storage of -15.2 mm per year for the period 2004-2015 (p-value < 0.01 in the Mann-Kendall test), which translates to a loss of 70.9 GT (gigatones) of water per decade. This suggests that, according to current estimates of glacier trends, the Brahmaputra River basin lost approximately as much land water as glacier water during the study period (with 67.5 GT lost due to glacier retreat). These numbers should be interpreted with an uncertainty at least as high as that of glacier retreat, estimated at up to ± 0.17 m water equivalent per year by Shean et al. (2020) (Table E1 of Appendix E), equivalent to ± 18.9 GT per decade. The drivers of these land water storage trends could be both natural climate variability and anthropogenic activities, and will be further explored in a future study. No significant storage trend is detected in the

https://doi.org/10.5194/egusphere-2025-5625
Preprint. Discussion started: 20 January 2026

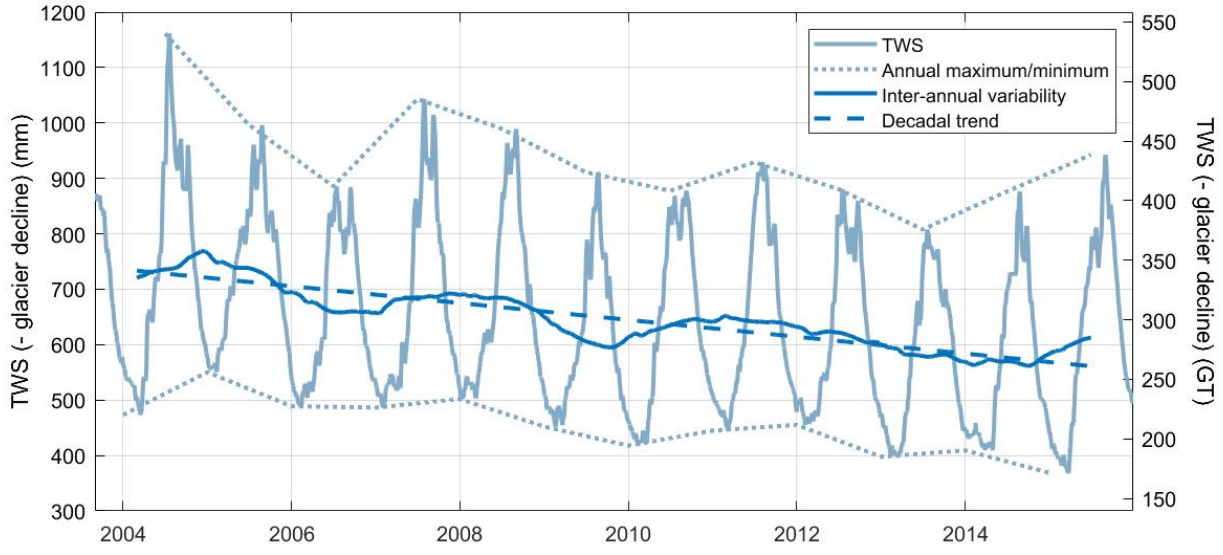

Figure 10. Basin averaged TWS (- glacier decline) for the Brahmaputra River basin from Approach #4. The left axis shows the TWS in mm, while the right axis shows the TWS in GT (gigatones).

SSM component, although dryness and wetness conditions could affect the SSM in the duration of the saturation period (to be assessed in a future study).

The TWS also displays a considerable inter-annual variability (std of 22 mm on detrended time series). For example, during the years 2007 and 2010, the basin gained 15.9 GT and 13.5 GT of water, respectively. In fact, these two periods have been reported as wet years in which extended flooding events occurred in the basin (Rao et al., 2020; Brakenridge). The impact of the wetness-dryness periods is found to have a stronger expression in the annual maximum values (std of 70 mm in detrended time series, upper pointy line in Fig. 10) than the minimum values (std of 26 mm in detrended time series, lower pointy line in Fig. 10), likely due to the contribution of the river water mass during high river flow events.

5 Conclusions

This study presents a daily-scale multi-variate Data Assimilation (DA) experiment for the Brahmaputra River basin, integrating TWS and SSM observations. In contrast to previous studies that assimilate GRACE TWS in a monthly timescale, the daily DA in this study enabled the assimilation of hydrological dynamics across multiple temporal scales, ranging from sub-monthly variability to decadal trends. The daily implementation also avoided model-observation temporal mismatch that typically requires complex smoothers or multi-step DA frameworks (Tian et al., 2017; Girotto et al., 2019; Tangdamrongsub et al., 2020), and thus allowed us to explore other aspects of the DA mechanism. The study pursued two main objectives: (i) investigating how different multi-variate DA approaches influence the DA mechanism and address limitations reported in the prior literature,

https://doi.org/10.5194/egusphere-2025-5625
Preprint. Discussion started: 20 January 2026

and (ii) generating improved land water storage estimates for the basin, allowing a refined analysis of its spatial and temporal hydrological variability.

For the first objective, we considered three existing and one new multi-variate DA approaches and analyzed their impact on the Kalman gain matrix and assimilation outcomes. Conventional uncertainty adjustment approaches (Tian et al., 2017) and observation space localization approaches (Girotto et al., 2019; Tangdamrongsub et al., 2020; Wongchuig et al., 2024) are useful to balance the influence of the different observations, but cannot fully avoid cross-variable interference, that is, TWS can strongly impact model SSM estimates and vice versa (especially when some of these variables are unconstrained). This is not necessarily a harmful effect and can be desirable in some circumstances to help address errors in observational datasets or in cases where TWS and SSM DA updates might enhance each other (see, e.g., Khaki and Awange, 2019; Khaki et al., 2019, 2020). However, previous studies in multi-variate land DA report that this cross-variable interference can lead to a diminished performance in multi-variate DA due to conflicting constraints or anti-correlated updates induced by the two observation sets (Tian et al., 2017; Girotto et al., 2019). As an example, in our study spurious decadal negative trends were introduced in the unconstrained SSM estimates when observation space localization was implemented.

To overcome this issue, we introduce a model space mixed covariance localization approach, which applies localization directly to the model covariance matrix. This method successfully regulates cross-variable influence for the first time, both in the uni-variate as well as the multi-variate DA, offering a way to address one of the most important challenges reported in multi-variate land DA literature so far. An additional interesting property of model space localization is its adequacy for assimilating spatially averaged (i.e., non-local) observations such as TWS (Campbell et al., 2010). The main drawback of this approach is that it requires explicit computation of the model covariance matrix and a Schur multiplication with the localization matrix, posing significant computational memory demands and motivating future work on its optimization.

Another approach that could possibly help avoid cross-variable influences is the application of a vertical observation space localization, aiming at concentrating the TWS update in the groundwater and the SSM update in the soil moisture. This approach was not considered in this study because the implementation of such localization is not straightforward, especially in the land hydrology system where water propagates vertically, and therefore water storage dynamics can be highly correlated across vertical storage components. Future studies could focus on proposing an adequate implementation of this approach and evaluating its potential benefits and limitations. An additional factor that could have an impact on the DA mechanism and has not been considered in this study is the extent of the observation error covariances. Although the impact of this factor has been evaluated in the context of uni-variate TWS DA experiments (e.g. Schumacher et al., 2016), more research is needed to determine its role in multi-variate land DA experiments.

For the second objective, validation against SPEI and in situ groundwater data shows that multi-variate DA substantially improves groundwater estimates, capturing both decadal trends and inter-annual variability and thus bringing the model closer to reality. SSM estimates also show notable improvements near mountainous regions, aligning more closely with independent models such as WaterGAP, which is found to be better adapted to high-mountain environments. A key limitation was identified in the lack of glacier representation in the W3RA model, which led to a misattribution of glacier melt signals to groundwater. In this study, these trends were removed after DA, but future research is required to address this aspect.

https://doi.org/10.5194/egusphere-2025-5625
Preprint. Discussion started: 20 January 2026

The enhanced DA time series enabled a robust characterization of hydrological variability in the Brahmaputra River basin, revealing a net water loss of 70.9 GT in 2005–2015 and pronounced inter-annual fluctuations. These refined estimates pave the way for further research into the drivers of land water variability and its expression in different hydrological compartments. Future work will explore the role of land water storage in flood generation and extend the analysis to the entire GRACE / GRACE-FO period (2002-2025), allowing for identification of bidecadal trends and an improved understanding of the dynamics of extreme events in the region.

Data availability. The results of the experiments performed in this study will be made openly available upon manuscript publication, doi 10.5281/zenodo.17591418.

Appendix A: Gap-filling algorithm

The monthly in situ groundwater level observations presented some minor gaps that needed to be filled. The following algorithm was found to perform satisfactorily for the study region. (This algorithm was applied to each in situ site independently).

1. Perform a Least-Squares regression to compute the mean and seasonality of the signal.
2. Fill the gaps with the values predicted by the Least-Squares fit.
3. Compute inter-annual variability of the signal, save it in auxiliary variable and deduce it from the signal.
4. Repeat step 1 and 2 over the signal with reduced inter-annual variability.
5. Add the inter-annual variability back to the signal.

This algorithm allows to fill the gaps in time series for which the seasonality can be approximately parameterized through a simple model, but the inter-annual variability is more difficult to parameterize due to its non-stationary nature. A PCA-based algorithm was also attempted, but did not work so well, likely due to the very heterogeneous groundwater dynamics in this region.

Appendix B: Detail of evaluation of DA experiments

Fig. B1 shows the impact of the different DA experiments on the sub-seasonal and sub-monthly variability of basin-averaged SSM and TWS, for years 2004 and 2005.

https://doi.org/10.5194/egusphere-2025-5625
Preprint. Discussion started: 20 January 2026

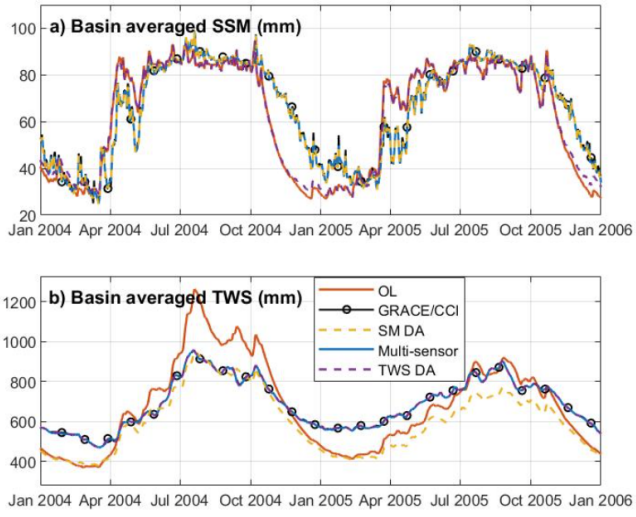

Figure B1. Impact of the different DA experiments on the sub-seasonal and sub-monthly variability of basin-averaged SSM (a) and TWS (b), for years 2004 and 2005.

Appendix C: Quantitative assessment of impact of DA settings on model estimates

Statistics of RMSD against assimilated data have been computed for the four DA tuning approaches considered in the main manuscript.

	RMSD (mm)			
	Multi-variate DA			
	Approach #1	**Approach #2**	**Approach #3**	**Approach #4**
TWS East	66.2	23.5	14.1	6.4
TWS West	84.1	38.5	21.9	9.5
TWS South	38.4	17.2	15.4	6.4
SSM average	8.1	9.2	4.1	3.8
SSM min	3.8	5.1	1.4	1.2
SSM max	18.7	19.7	9.1	8.7

Table C1. RMSD of model estimates (OL, SSM DA, multi-variate DA and TWS DA) with respect to assimilated data. SSM min and SSM max refer to the minimum and maximum RMSD values across the $0.25^\circ \times 0.25^\circ$ tiles.

Additionally, the following plot shows the TWS times series of multi-variate DA with no DA tuning (approach #1). The time series reveal sharp spikes introduced by the SSM DA that are not observed in the GRACE TWS. The spikes are especially strong in the dryer periods (i.e., 2013-2015).

https://doi.org/10.5194/egusphere-2025-5625
Preprint. Discussion started: 20 January 2026

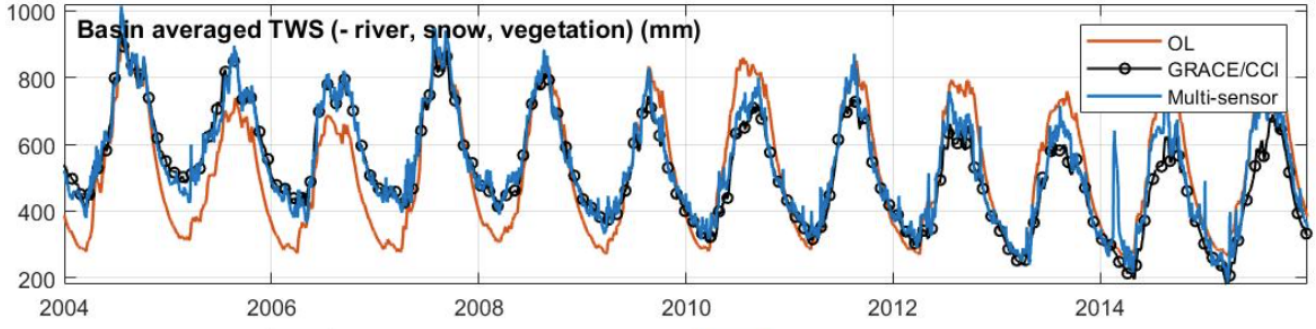

Figure C1. TWS time series for OL and multi-variate DA with no DA tuning approach. GRACE TWS is shown in black as a reference.

Appendix D: Evaluating the impact of additional DA setting parameters

In the main manuscript we evaluate the impact of localization and uncertainty adjustment settings on the multi-variate DA results. Here we present some additional figures showing the impact of TWS detrending and including river storage in the DA update process.

Assimilating detrended TWS observations was found to lead to smoother spatial update patterns (Fig. D1). This suggests that the ensemble statistics perform better at distributing the updates horizontally when there are no large systematic differences between model and observations.

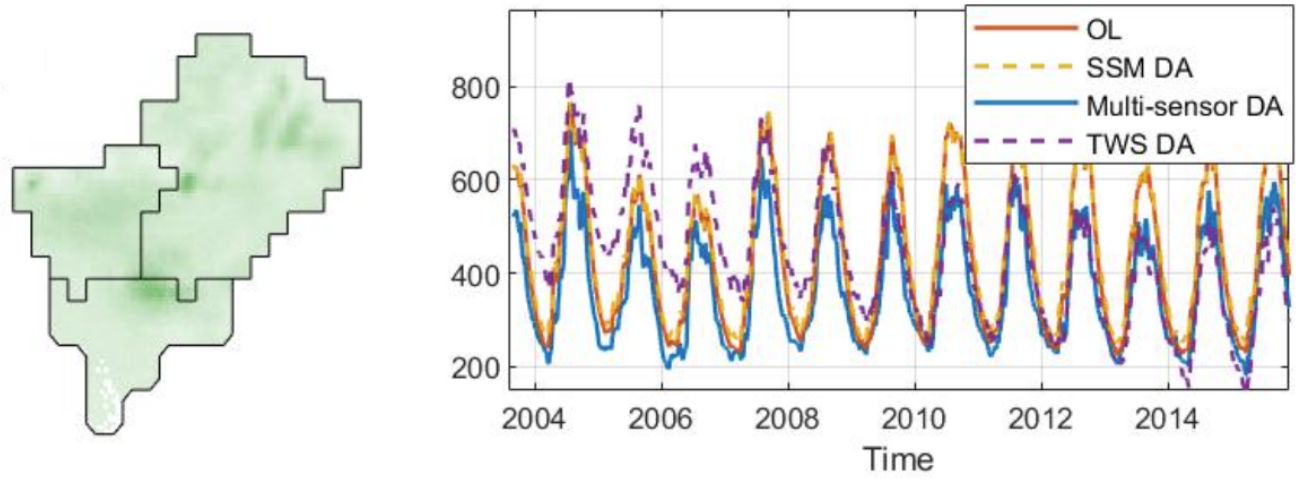

Figure D1. Spatial groundwater disaggregation and sub-basin averaged groundwater time series, when detrended TWS is assimilated.

Another alternative experiment was also performed by **including the river storage compartment in the DA update process**. For this experiment, the decadal trends were removed from the GRACE TWS time series to avoid transferring these into

https://doi.org/10.5194/egusphere-2025-5625
Preprint. Discussion started: 20 January 2026

the river storage estimates. The validation was performed in terms of seasonal and sub-seasonal dynamics, and revealed degradations in the main river branch estimates in the sub-seasonal timescale with minor improvements in the seasonal timescale (Fig. D2). Additionally, it was already reported by Retegui-Schiettekatte et al. (2025a) (Fig. S8) that including the snow component in the update process can also introduce unrealistic anomalies in the snow estimates. Because of this, the two components were excluded from the DA update process in the experiments presented in the main manuscript.

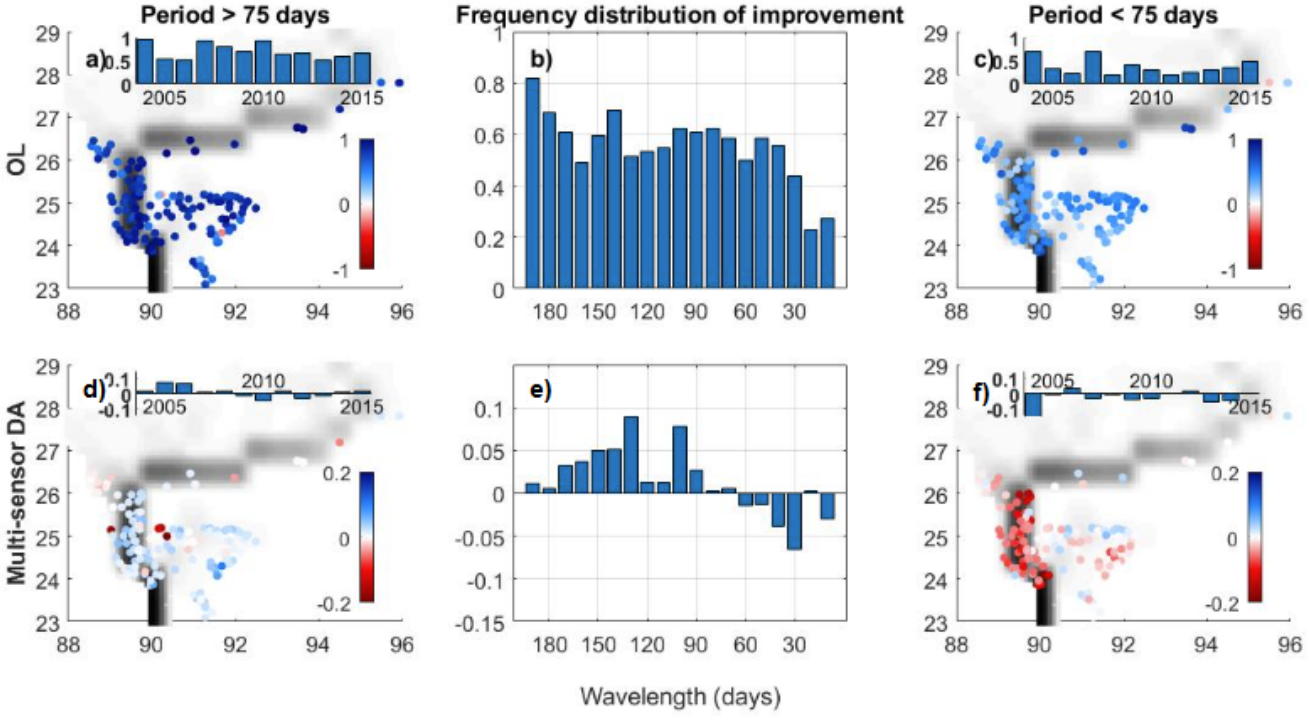

Figure D2. Validation of distributed water storage estimates in terms of correlation coefficient, in an alternative DA experiment where river storage was updated as part of the DA update process.

https://doi.org/10.5194/egusphere-2025-5625
Preprint. Discussion started: 20 January 2026

Appendix E: Additional groundwater evaluation

Figure E1 reproduces the groundwater validation of the main manuscript while including the SM DA and TWS DA experiment outputs. The results support the conclusions of Section 4.3.1 of the main manuscript that multi-sensor DA fully captures the benefits of TWS DA on groundwater dynamics.

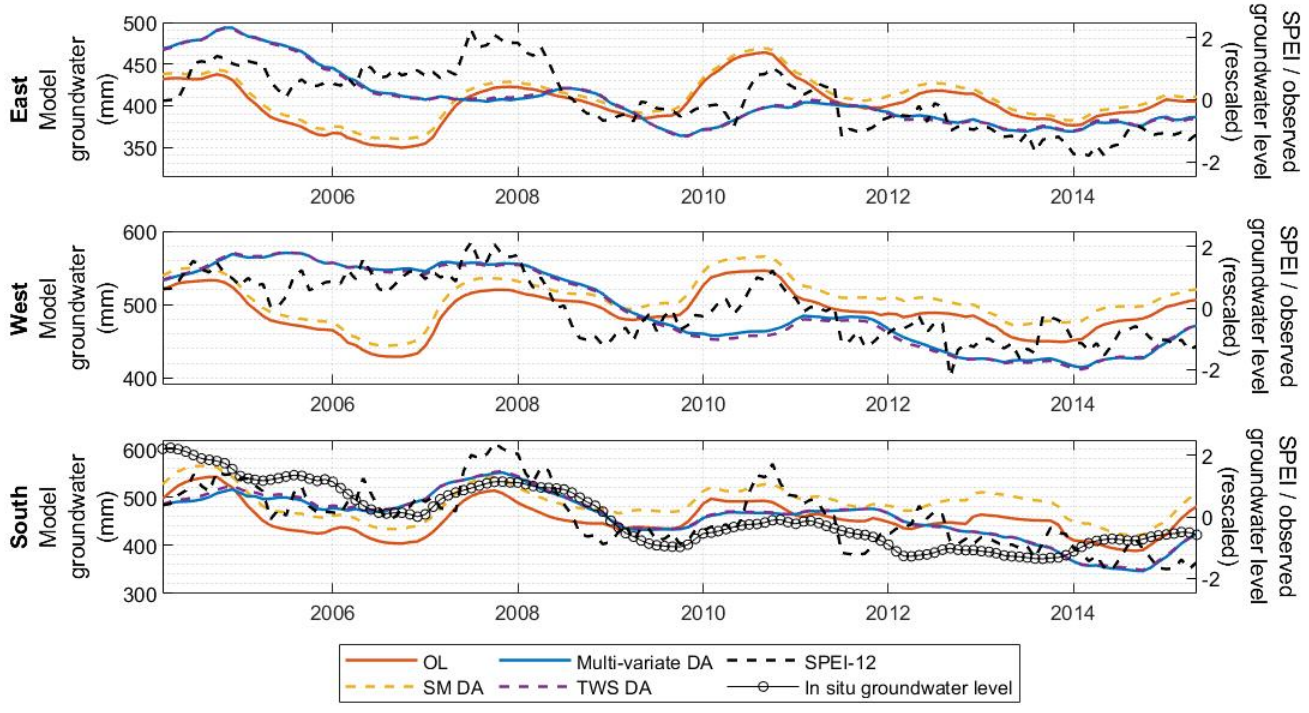

Figure E1. Inter-annual deep water time series from OL, SM DA, multi-sensor DA and TWS DA experiments. SPEI time series and groundwater level observations are shown for comparison (rescaled, on the right side axis).

Fig. E2 shows a comparison modeled groundwater storage and in situ groundwater levels, including seasonality. The picture shows that DA mainly modifies the model estimates in terms of seasonality amplitude and inter-annual variability.

https://doi.org/10.5194/egusphere-2025-5625
Preprint. Discussion started: 20 January 2026

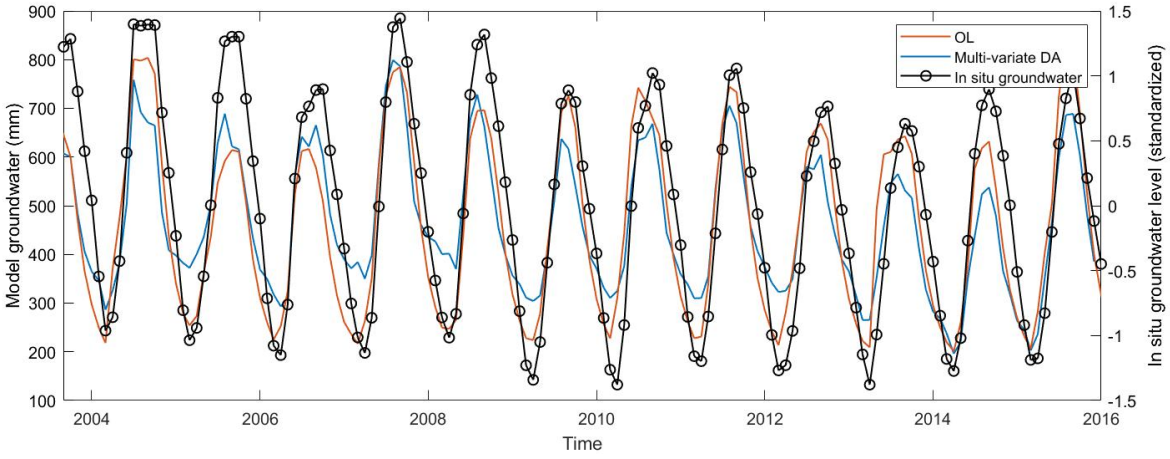

Figure E2. Model (OL and multi-variate DA) as well as in situ groundwater time series averaged for the South sub-basin.

Below are different glacier trends proposed by studies in literature for glacier in the Brahmaputra River basin (Table E1). While in the main manuscript a conservative approach is chosen by taking the largest glacier trends, here the process is repeated with smaller trends (-0.50 m w.e., water equivalent, per year for the East sub-basin and -0.43 mm w.e. per year for the West sub-basin). The statistics, shown on Table E2, show that multi-variate DA leads to significant improvements even when smaller glacier trends are considered.

	Glacier trends (m w.e. per year)	
	Nyainqentanglha (East sub-basin)	Buthan (West sub-basin)
Brun et al. (2017)	-0.63	-0.43
Shean et al. (2020)	-0.50 $\pm$ 0.15	-0.55 $\pm$ 0.17
Hugonnet et al. (2021)	(not explicitly provided)	-0.49 $\pm$ 0.10 (Vishwakarma et al., 2022)
Here used	-0.63	-0.55

Table E1. Glacier trends within the Brahmaputra River basin, as reported in previous literature based on stereo satellite imagery. "w.e." = water equivalent.

Appendix F: Additional SSM evaluation

Differences between W3RA and WaterGAP SSM could originate from the difference in SSM layer depths. Indeed, the W3RA SSM average field capacity over the region is around 94 mm, while the WaterGAP average field capacity seems to be around 120 mm (see Fig. F1a). To exclude this possibility, we have repeated the comparison by considering all the soil water storage

https://doi.org/10.5194/egusphere-2025-5625
Preprint. Discussion started: 20 January 2026

	OL	Multi-variate DA
East sub-basin (ref. SPEI)	0.15	0.67
West sub-basin (ref. SPEI)	0.24	0.79
South sub-basin (ref. SPEI)	0.57	0.81
South sub-basin (ref. BWDB)	0.49	0.73

Table E2. Correlation coefficient between modeled and independent groundwater storage variability estimation, when considering smaller glacier trends. All correlations are significant with p-value < 0.01.

compartments of W3RA, that is, topsoil, shallow soil and deep soil, with an average field capacity of 452 mm over the region. The results still show that the W3RA SSM tends to saturate and decay earlier than the WaterGAP SSM (Fig. F1a) and present especially high discrepancies with WaterGAP in mountain areas (see Fig. F1b). This confirms that the differences might originate from the model structure rather than the SSM layer depth.

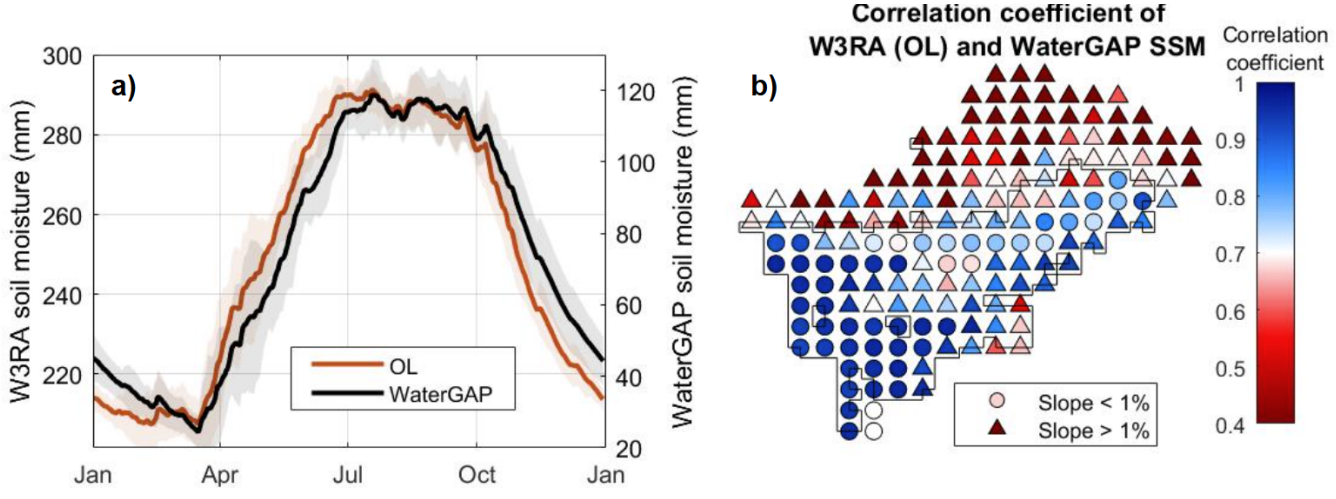

Figure F1. a) SSM seasonality of W3RA OL (including deep soil) and WaterGAP. b) Distributed map of correlation coefficient of W3RA (OL, including deep soil) and WaterGAP, shown for the WaterGAP $0.5° \times 0.5°$ tiles. The black outline in b) indicates the area where SSM observations were assimilated.

765 *Author contributions.* CRediT statement. Conceptualization: LR, MG, MS, EF; Data curation: LR, EF; Formal Analysis: LR, MG, EF; Funding acquisition: LR, MG, EF; Investigation: LR, MG, MSh, EF; Methodology: LR, MG, EF; Project administration: LR, MG, EF; Resources: MG, MS, HM, MSh, EF; Software: LR, MS; Supervision: MG, HM, EF; Validation: LR, MG, HM, MSh, EF; Visualization: LR, MG, MS; Writing – original draft: LR, MG, EF; Writing – review & editing: LR, MG, MS, HM, MSh, EF

https://doi.org/10.5194/egusphere-2025-5625
Preprint. Discussion started: 20 January 2026

Competing interests. The authors declare that they have no conflict of interest.

Acknowledgements. This work was supported by the Danmarks Frie Forskningsfond (DFF) (10.46540/2035-00247B) through the DANSk-LSM project. A research visit by Leire Retegui-Schiettekatte at the University of California Berkeley was partially supported by the Otto Mønsted Foundation (Denmark) as well as the EliteForsk travel grant (Ministry of Higher Education and Science, Denmark). Ehsan Forootan acknowledges the funding from the DFF Thematic-Green SFAS project (10.46540/4307-00146B). Some of the experiments of this study were carried out using High Performance Computing resources provided by the Danish e-infrastructure Consortium (DeiC).

The GRACE ITSG-2018 product Mayer-Gürr et al. (2018); Kvas et al. (2019) is provided openly by the Institute of Geodesy of the Graz University of Technology (https://www.tugraz.at/institute/ifg/downloads/gravity-field-models/itsg-grace2018#c194122). The SSM data are provided by the European Space Agency Climate Change Initiative (Gruber et al., 2019; Dorigo et al., 2017; Preimesberger et al., 2021, ESA CCI SSM,) (https://climate.esa.int/en/projects/soil-moisture/). The original codes for the World Wide Water Resources Assessment model (W3RA, Van Dijk (2010); van Dijk et al. (2013)) were kindly provided by Albert I.J.M. van Dijk, and the model was downscaled at by the Geodesy Group at Aalborg University. ERA5 Hersbach and Dee (2016) and ERA5-Land Muñoz Sabater et al. (2019) data were downloaded from the Copernicus Climate Change Service (2023). The watershed definitions of WGHM are openly provided in Müller Schmied and Schiebener (2022). The slope data used to interpret the SSM validation was derived from (**?**) (https://www.earthenv.org/topography). The SPEI-12 time series used to validate groundwater were derived from (Beguería et al., 2014) and are available in the Global Drought Monitor (khttps://spei.csic.es/map/maps.html#months=1#month=7#year=2025).

https://doi.org/10.5194/egusphere-2025-5625
Preprint. Discussion started: 20 January 2026

References

Numerical Methods, in: Introduction to Bayesian Statistics, edited by Koch, K.-R., pp. 193–234, Springer, Berlin, Heidelberg, ISBN 978-3-540-72726-2, https://doi.org/10.1007/978-3-540-72726-2_6, 2007.

Ahmad, J. A., Forman, B. A., Getirana, A., and Kumar, S. V.: Influence of SMAP soil moisture retrieval assimilation on runoff estimation across South Asia, Journal of Hydrology, 639, 131 550, https://doi.org/10.1016/j.jhydrol.2024.131550, 2024.

Alam, S., Ali, M. M., Rahaman, A. Z., and Islam, Z.: Multi-model ensemble projection of mean and extreme streamflow of Brahmaputra River Basin under the impact of climate change, Journal of Water and Climate Change, 12, 2026–2044, https://doi.org/10.2166/wcc.2021.286, 2021.

Amatulli, G., Domisch, S., Tuanmu, M.-N., Parmentier, B., Ranipeta, A., Malczyk, J., and Jetz, W.: A suite of global, cross-scale topographic variables for environmental and biodiversity modeling, Sci Data, 5, 180 040, https://doi.org/10.1038/sdata.2018.40, publisher: Nature Publishing Group, 2018.

Beguería, S., Vicente-Serrano, S. M., Reig, F., and Latorre, B.: Standardized precipitation evapotranspiration index (SPEI) revisited: parameter fitting, evapotranspiration models, tools, datasets and drought monitoring, International Journal of Climatology, 34, 3001–3023, https://doi.org/10.1002/joc.3887, _eprint: https://rmets.onlinelibrary.wiley.com/doi/pdf/10.1002/joc.3887, 2014.

Blyverket, J., Hamer, P. D., Bertino, L., Albergel, C., Fairbairn, D., and Lahoz, W. A.: An Evaluation of the EnKF vs. EnOI and the Assimilation of SMAP, SMOS and ESA CCI Soil Moisture Data over the Contiguous US, Remote Sensing, 11, 478, https://doi.org/10.3390/rs11050478, publisher: Multidisciplinary Digital Publishing Institute, 2019.

Boergens, E., Kvas, A., Eicker, A., Dobslaw, H., Schawohl, L., Dahle, C., Murböck, M., and Flechtner, F.: Uncertainties of GRACE-Based Terrestrial Water Storage Anomalies for Arbitrary Averaging Regions, Journal of Geophysical Research: Solid Earth, 127, e2021JB022 081, https://doi.org/10.1029/2021JB022081, 2022.

Bolaños Chavarría, S., Werner, M., Salazar, J. F., and Betancur Vargas, T.: Benchmarking global hydrological and land surface models against GRACE in a medium-sized tropical basin, Hydrology and Earth System Sciences, 26, 4323–4344, https://doi.org/10.5194/hess-26-4323-2022, 2022.

Brakenridge, G.: Global Active Archive of Large Flood Events. Dartmouth Flood Observatory, University of Colorado, USA. http://floodobservatory.colorado.edu/ Archives/ (Accessed 1 October 2023).

Brammer, H.: Floods in Bangladesh: Geographical Background to the 1987 and 1988 Floods, The Geographical Journal, 156, 12–22, https://doi.org/10.2307/635431, 1990.

Brocca, L., Melone, F., Moramarco, T., Wagner, W., Naeimi, V., Bartalis, Z., and Hasenauer, S.: Improving runoff prediction through the assimilation of the ASCAT soil moisture product, Hydrology and Earth System Sciences, 14, 1881–1893, https://doi.org/10.5194/hess-14-1881-2010, 2010.

Brocca, L., Ciabatta, L., Massari, C., Camici, S., and Tarpanelli, A.: Soil Moisture for Hydrological Applications: Open Questions and New Opportunities, Water, 9, 140, https://doi.org/10.3390/w9020140, number: 2 Publisher: Multidisciplinary Digital Publishing Institute, 2017.

Brown, S., Nicholls, R. J., Lázár, A. N., Hornby, D. D., Hill, C., Hazra, S., Appeaning Addo, K., Haque, A., Caesar, J., and Tompkins, E. L.: What are the implications of sea-level rise for a 1.5, 2 and 3 °C rise in global mean temperatures in the Ganges-Brahmaputra-Meghna and other vulnerable deltas?, Reg Environ Change, 18, 1829–1842, https://doi.org/10.1007/s10113-018-1311-0, 2018.

Brun, F., Berthier, E., Wagnon, P., Kääb, A., and Treichler, D.: A spatially resolved estimate of High Mountain Asia glacier mass balances from 2000 to 2016, Nature Geosci, 10, 668–673, https://doi.org/10.1038/ngeo2999, publisher: Nature Publishing Group, 2017.

https://doi.org/10.5194/egusphere-2025-5625
Preprint. Discussion started: 20 January 2026

Burgers, G., Leeuwen, P. J. v., and Evensen, G.: Analysis Scheme in the Ensemble Kalman Filter, Monthly Weather Review, 126, 1719–1724, https://doi.org/10.1175/1520-0493(1998)126<1719:ASITEK>2.0.CO;2, 1998.

Campbell, W. F., Bishop, C. H., and Hodyss, D.: Vertical Covariance Localization for Satellite Radiances in Ensemble Kalman Filters, Monthly Weather Review, 138, 282–290, https://doi.org/10.1175/2009MWR3017.1, publisher: American Meteorological Society Section: Monthly Weather Review, 2010.

Chen, F., Crow, W. T., Starks, P. J., and Moriasi, D. N.: Improving hydrologic predictions of a catchment model via assimilation of surface soil moisture, Advances in Water Resources, 34, 526–536, https://doi.org/10.1016/j.advwatres.2011.01.011, 2011.

Chen, X., Long, D., Hong, Y., Zeng, C., and Yan, D.: Improved modeling of snow and glacier melting by a progressive two-stage calibration strategy with GRACE and multisource data: How snow and glacier meltwater contributes to the runoff of the Upper Brahmaputra River basin?, Water Resources Research, 53, 2431–2466, https://doi.org/10.1002/2016WR019656, _eprint: https://agupubs.onlinelibrary.wiley.com/doi/pdf/10.1002/2016WR019656, 2017.

Commission, C. W.: Brahmaputra Basin Version 2.0, Tech. rep., 2014.

Crow, W. T. and Ryu, D.: A new data assimilation approach for improving runoff prediction using remotely-sensed soil moisture retrievals, Hydrology and Earth System Sciences, 13, 1–16, https://doi.org/10.5194/hess-13-1-2009, publisher: Copernicus GmbH, 2009.

Das, P. and Kumar, M.: Climate Change and Sustainable Management of the Rivers System with Special Reference to the Brahmaputra River, in: Water Conservation, Recycling and Reuse: Issues and Challenges, edited by Singh, R. P., Kolok, A. S., and Bartelt-Hunt, S. L., pp. 95–106, Springer, Singapore, ISBN 978-981-13-3179-4, https://doi.org/10.1007/978-981-13-3179-4_5, 2019.

De Lannoy, G. J. M., Bechtold, M., Busschaert, L., Heyvaert, Z., Modanesi, S., Dunmire, D., Lievens, H., Getirana, A., and Massari, C.: Contributions of Irrigation Modeling, Soil Moisture and Snow Data Assimilation to High-Resolution Water Budget Estimates Over the Po Basin: Progress Towards Digital Replicas, Journal of Advances in Modeling Earth Systems, 16, e2024MS004 433, https://doi.org/10.1029/2024MS004433, _eprint: https://onlinelibrary.wiley.com/doi/pdf/10.1029/2024MS004433, 2024.

Dorigo, W., Wagner, W., Albergel, C., Albrecht, F., Balsamo, G., Brocca, L., Chung, D., Ertl, M., Forkel, M., Gruber, A., Haas, E., Hamer, P. D., Hirschi, M., Ikonen, J., de Jeu, R., Kidd, R., Lahoz, W., Liu, Y. Y., Miralles, D., Mistelbauer, T., Nicolai-Shaw, N., Parinussa, R., Pratola, C., Reimer, C., van der Schalie, R., Seneviratne, S. I., Smolander, T., and Lecomte, P.: ESA CCI Soil Moisture for improved Earth system understanding: State-of-the art and future directions, Remote Sensing of Environment, 203, 185–215, https://doi.org/10.1016/j.rse.2017.07.001, 2017.

Dube, T., Seaton, D., Shoko, C., and Mbow, C.: Advancements in earth observation for water resources monitoring and management in Africa: A comprehensive review, Journal of Hydrology, 623, 129 738, https://doi.org/https://doi.org/10.1016/j.jhydrol.2023.129738, 2023.

Dutta, P., Hinge, G., Marak, J. D. K., and Sarma, A. K.: Future climate and its impact on streamflow: a case study of the Brahmaputra river basin, Model. Earth Syst. Environ., 7, 2475–2490, https://doi.org/10.1007/s40808-020-01022-2, 2021.

Döll, P., Kaspar, F., and Lehner, B.: A global hydrological model for deriving water availability indicators: model tuning and validation, Journal of Hydrology, 270, 105–134, https://doi.org/10.1016/S0022-1694(02)00283-4, 2003.

Eicker, A., Schumacher, M., Kusche, J., Döll, P., and Schmied, H. M.: Calibration/Data Assimilation Approach for Integrating GRACE Data into the WaterGAP Global Hydrology Model (WGHM) Using an Ensemble Kalman Filter: First Results, Surv Geophys, 35, 1285–1309, https://doi.org/10.1007/s10712-014-9309-8, 2014.

Eicker, A., Forootan, E., Springer, A., Longuevergne, L., and Kusche, J.: Does GRACE see the terrestrial water cycle "intensifying"?, Journal of Geophysical Research: Atmospheres, 121, 733–745, https://doi.org/10.1002/2015JD023808, 2016.

https://doi.org/10.5194/egusphere-2025-5625
Preprint. Discussion started: 20 January 2026

Entekhabi, D., Njoku, E. G., O'Neill, P. E., Kellogg, K. H., Crow, W. T., Edelstein, W. N., Entin, J. K., Goodman, S. D., Jackson, T. J., Johnson, J., Kimball, J., Piepmeier, J. R., Koster, R. D., Martin, N., McDonald, K. C., Moghaddam, M., Moran, S., Reichle, R., Shi, J. C., Spencer, M. W., Thurman, S. W., Tsang, L., and Van Zyl, J.: The Soil Moisture Active Passive (SMAP) Mission, Proceedings of the IEEE, 98, 704–716, https://doi.org/10.1109/JPROC.2010.2043918, 2010.

Evensen, G.: Sequential data assimilation with a nonlinear quasi-geostrophic model using Monte Carlo methods to forecast error statistics, Journal of Geophysical Research: Oceans, 99, 10 143–10 162, https://doi.org/10.1029/94JC00572, _eprint: https://onlinelibrary.wiley.com/doi/pdf/10.1029/94JC00572, 1994.

Evensen, G.: The Ensemble Kalman Filter: theoretical formulation and practical implementation, Ocean Dynamics, 53, 343–367, https://doi.org/10.1007/s10236-003-0036-9, 2003.

Flechtner, F., Morton, P., Watkins, M., and Webb, F.: Status of the GRACE Follow-On Mission, in: Gravity, Geoid and Height Systems, edited by Marti, U., pp. 117–121, Springer International Publishing, Cham, ISBN 978-3-319-10837-7, https://doi.org/10.1007/978-3-319-10837-7_15, 2014.

Forootan, E. and Kusche, J.: Separation of global time-variable gravity signals into maximally independent components, Journal of Geodesy, 86, 477–497, https://doi.org/0.1007/s00190-011-0532-5, 2012.

Gain, A. K. and Wada, Y.: Assessment of Future Water Scarcity at Different Spatial and Temporal Scales of the Brahmaputra River Basin, Water Resour Manage, 28, 999–1012, https://doi.org/10.1007/s11269-014-0530-5, 2014.

Gain, A. K., Immerzeel, W. W., Sperna Weiland, F. C., and Bierkens, M. F. P.: Impact of climate change on the stream flow of the lower Brahmaputra: trends in high and low flows based on discharge-weighted ensemble modelling, Hydrology and Earth System Sciences, 15, 1537–1545, https://doi.org/10.5194/hess-15-1537-2011, publisher: Copernicus GmbH, 2011.

Gaspari, G. and Cohn, S. E.: Construction of correlation functions in two and three dimensions, Quarterly Journal of the Royal Meteorological Society, 125, 723–757, https://doi.org/10.1002/qj.49712555417, 1999.

Gerdener, H., Kusche, J., Schulze, K., Döll, P., and Klos, A.: The global land water storage data set release 2 (GLWS2.0) derived via assimilating GRACE and GRACE-FO data into a global hydrological model, J Geod, 97, 73, https://doi.org/10.1007/s00190-023-01763-9, 2023.

Getirana, A., Rodell, M., Kumar, S., Beaudoing, H., Arsenault, K., Zaitchik, B., Save, H., and Bettadpur, S.: GRACE improves seasonal groundwater forecast initialization over the U.S., J Hydrometeorol., 21(1), 59–71, https://doi.org/doi: 10.1175/jhm-d-19-0096.1, 2020.

Getirana, A., Kumar, S., and Rodell, M.: Inconsistencies in GRACE-Based Groundwater Storage Estimation—A Call for a Proper Use of Land Surface Models, Geophysical Research Letters, 52, e2025GL119 197, https://doi.org/10.1029/2025GL119197, _eprint: https://agupubs.onlinelibrary.wiley.com/doi/pdf/10.1029/2025GL119197, 2025.

Girotto, M., De Lannoy, G. J. M., Reichle, R. H., and Rodell, M.: Assimilation of gridded terrestrial water storage observations from GRACE into a land surface model, Water Resources Research, 52, 4164–4183, https://doi.org/10.1002/2015WR018417, 2016.

Girotto, M., De Lannoy, G. J., Reichle, R. H., Rodell, M., Draper, C., Bhanja, S. N., and Mukherjee, A.: Benefits and pitfalls of GRACE data assimilation: A case study of terrestrial water storage depletion in India, Geophysical research letters, 44, 4107–4115, https://doi.org/10.1002/2017GL072994, 2017.

Girotto, M., Reichle, R. H., Rodell, M., Liu, Q., Mahanama, S., and De Lannoy, G. J. M.: Multi-sensor assimilation of SMOS brightness temperature and GRACE terrestrial water storage observations for soil moisture and shallow groundwater estimation, Remote Sensing of Environment, 227, 12–27, https://doi.org/10.1016/j.rse.2019.04.001, 2019.

https://doi.org/10.5194/egusphere-2025-5625
Preprint. Discussion started: 20 January 2026

Gogoi, P. P., Vinoj, V., Landu, K., and Phukon, P.: The changing characteristics of rainfall over the Brahmaputra Basin during 1998–2018, Quarterly Journal of the Royal Meteorological Society, 149, 608–620, https://doi.org/10.1002/qj.4427, publisher: John Wiley & Sons, Ltd, 2023.

Gruber, A., Scanlon, T., van der Schalie, R., Wagner, W., and Dorigo, W.: Evolution of the ESA CCI Soil Moisture climate data records and their underlying merging methodology, Earth System Science Data, 11, 717–739, https://doi.org/10.5194/essd-11-717-2019, 2019.

Gruber, A., De Lannoy, G., Albergel, C., Al-Yaari, A., Brocca, L., Calvet, J. C., Colliander, A., Cosh, M., Crow, W., Dorigo, W., Draper, C., Hirschi, M., Kerr, Y., Konings, A., Lahoz, W., McColl, K., Montzka, C., Muñoz-Sabater, J., Peng, J., Reichle, R., Richaume, P., Rüdiger, C., Scanlon, T., van der Schalie, R., Wigneron, J. P., and Wagner, W.: Validation practices for satellite soil moisture retrievals: What are (the) errors?, Remote Sensing of Environment, 244, 111 806, https://doi.org/10.1016/j.rse.2020.111806, 2020.

Hamill, T. M., Whitaker, J. S., and Snyder, C.: Distance-Dependent Filtering of Background Error Covariance Estimates in an Ensemble Kalman Filter, Monthly Weather Review, 129, 2776–2790, https://doi.org/10.1175/1520-0493(2001)129<2776:DDFOBE>2.0.CO;2, 2001.

Hersbach, H. and Dee, D.: ERA5 reanalysis is in production, ECMWF newsletter, 147, 5–6, https://doi.org/10.24381/cds.adbb2d47, 2016.

Houtekamer, P. L. and Mitchell, H. L.: Data Assimilation Using an Ensemble Kalman Filter Technique, Monthly Weather Review, 126, 796–811, https://doi.org/10.1175/1520-0493(1998)126<0796:DAUAEK>2.0.CO;2, publisher: American Meteorological Society Section: Monthly Weather Review, 1998.

Houtekamer, P. L. and Mitchell, H. L.: A Sequential Ensemble Kalman Filter for Atmospheric Data Assimilation, Monthly Weather Review, 129, 123–137, https://doi.org/10.1175/1520-0493(2001)129<0123:ASEKFF>2.0.CO;2, 2001.

Hugonnet, R., McNabb, R., Berthier, E., Menounos, B., Nuth, C., Girod, L., Farinotti, D., Huss, M., Dussaillant, I., Brun, F., and Kääb, A.: Accelerated global glacier mass loss in the early twenty-first century, Nature, 592, 726–731, https://doi.org/10.1038/s41586-021-03436-z, publisher: Nature Publishing Group, 2021.

Immerzeel, W.: Historical trends and future predictions of climate variability in the Brahmaputra basin, International Journal of Climatology, 28, 243–254, https://doi.org/10.1002/joc.1528, 2008.

Intergovernmental Panel On Climate Change (IPCC): Climate Change 2022 – Impacts, Adaptation and Vulnerability: Working Group II Contribution to the Sixth Assessment Report of the Intergovernmental Panel on Climate Change, Cambridge University Press, 1 edn., ISBN 978-1-009-32584-4, https://doi.org/10.1017/9781009325844, 2023.

Kauffeldt, A., Wetterhall, F., Pappenberger, F., Salamon, P., and Thielen, J.: Technical review of large-scale hydrological models for implementation in operational flood forecasting schemes on continental level, Environmental Modelling & Software, 75, 68–76, https://doi.org/https://doi.org/10.1016/j.envsoft.2015.09.009, 2016.

Kerr, Y. H., Waldteufel, P., Wigneron, J.-P., Delwart, S., Cabot, F., Boutin, J., Escorihuela, M.-J., Font, J., Reul, N., Gruhier, C., Juglea, S. E., Drinkwater, M. R., Hahne, A., Martín-Neira, M., and Mecklenburg, S.: The SMOS Mission: New Tool for Monitoring Key Elements ofthe Global Water Cycle, Proceedings of the IEEE, 98, 666–687, https://doi.org/10.1109/JPROC.2010.2043032, 2010.

Khaki, M. and Awange, J.: The application of multi-mission satellite data assimilation for studying water storage changes over South America, Science of The Total Environment, 647, 1557–1572, https://doi.org/10.1016/j.scitotenv.2018.08.079, 2019.

Khaki, M., Hoteit, I., Kuhn, M., Forootan, E., and Awange, J.: Assessing data assimilation frameworks for using multi-mission satellite products in a hydrological context, Science of The Total Environment, 647, 1031–1043, https://doi.org/10.1016/j.scitotenv.2018.08.032, 2019.

https://doi.org/10.5194/egusphere-2025-5625
Preprint. Discussion started: 20 January 2026

Khaki, M., Hendricks Franssen, H.-J., and Han, S. C.: Multi-mission satellite remote sensing data for improving land hydrological models via data assimilation, Sci Rep, 10, 18 791, https://doi.org/10.1038/s41598-020-75710-5, publisher: Nature Publishing Group, 2020.

Khandu, Forootan, E., Schumacher, M., Awange, J. L., and Schmied, H. M.: Exploring the influence of precipitation extremes and human water use on total water storage (TWS) changes in the Ganges-Brahmaputra-Meghna River Basin, Water Resources Research, 52, 2240–2258, https://doi.org/10.1002/2015WR018113, publisher: John Wiley & Sons, Ltd, 2016.

Kirby, M. and Mainuddin, M.: The impact of climate change, population growth and development on sustainable water security in Bangladesh to 2100, Sci Rep, 12, 22 344, https://doi.org/10.1038/s41598-022-26807-6, publisher: Nature Publishing Group, 2022.

Kusche, J., Eicker, A., Forootan, E., Springer, A., and Longuevergne, L.: Mapping probabilities of extreme continental water storage changes from space gravimetry, Geophysical Research Letters, 43, 8026–8034, https://doi.org/10.1002/2016GL069538, 2016.

Kvas, A., Behzadpour, S., Ellmer, M., Klinger, B., Strasser, S., Zehentner, N., and Mayer-Gürr, T.: ITSG-Grace2018: Overview and Evaluation of a New GRACE-Only Gravity Field Time Series, Journal of Geophysical Research: Solid Earth, 124, 9332–9344, https://doi.org/10.1029/2019JB017415, 2019.

Lei, L., Whitaker, J. S., and Bishop, C.: Improving Assimilation of Radiance Observations by Implementing Model Space Localization in an Ensemble Kalman Filter, Journal of Advances in Modeling Earth Systems, 10, 3221–3232, https://doi.org/10.1029/2018MS001468, _eprint: https://agupubs.onlinelibrary.wiley.com/doi/pdf/10.1029/2018MS001468, 2018.

Li, B., Rodell, M., Kumar, S., Beaudoing, H. K., Getirana, A., Zaitchik, B. F., de Goncalves, L. G., Cossetin, C., Bhanja, S., Mukherjee, A., Tian, S., Tangdamrongsub, N., Long, D., Nanteza, J., Lee, J., Policelli, F., Goni, I. B., Daira, D., Bila, M., de Lannoy, G., Mocko, D., Steele-Dunne, S. C., Save, H., and Bettadpur, S.: Global GRACE Data Assimilation for Groundwater and Drought Monitoring: Advances and Challenges, Water Resources Research, 55, 7564–7586, https://doi.org/10.1029/2018WR024618, 2019.

Lutz, A. F., Immerzeel, W. W., Shrestha, A. B., and Bierkens, M. F. P.: Consistent increase in High Asia's runoff due to increasing glacier melt and precipitation, Nature Clim Change, 4, 587–592, https://doi.org/10.1038/nclimate2237, publisher: Nature Publishing Group, 2014.

Maina, F. Z., Getirana, A., Kumar, S. V., Saharia, M., Biswas, N. K., McLarty, S., and Appana, R.: Irrigation-driven groundwater depletion in the Ganges-Brahmaputra basin decreases the streamflow in the Bay of Bengal, Commun Earth Environ, 5, 169, https://doi.org/10.1038/s43247-024-01348-0, publisher: Nature Publishing Group, 2024.

Masood, M., Yeh, P. J.-F., Hanasaki, N., and Takeuchi, K.: Model study of the impacts of future climate change on the hydrology of Ganges–Brahmaputra–Meghna basin, Hydrology and Earth System Sciences, 19, 747–770, https://doi.org/10.5194/hess-19-747-2015, publisher: Copernicus GmbH, 2015.

Massari, C., Brocca, L., Tarpanelli, A., and Moramarco, T.: Data Assimilation of Satellite Soil Moisture into Rainfall-Runoff Modelling: A Complex Recipe?, Remote Sensing, 7, 11 403–11 433, https://doi.org/10.3390/rs70911403, number: 9 Publisher: Multidisciplinary Digital Publishing Institute, 2015.

Matgen, P., Fenicia, F., Heitz, S., Plaza, D., de Keyser, R., Pauwels, V. R. N., Wagner, W., and Savenije, H.: Can ASCAT-derived soil wetness indices reduce predictive uncertainty in well-gauged areas? A comparison with *in situ* observed soil moisture in an assimilation application, Advances in Water Resources, 44, 49–65, https://doi.org/10.1016/j.advwatres.2012.03.022, 2012.

Mayer-Gürr, T., Behzadpur, S., Ellmer, M., Kvas, A., Klinger, B., Strasser, S., and Zehentner, N.: ITSG-Grace2018 - Monthly, Daily and Static Gravity Field Solutions from GRACE, https://doi.org/10.5880/ICGEM.2018.003, 2018.

Medhi, S., Choudhury, R., Sharma, P., and Nath, B.: Groundwater Dynamics in the Middle Brahmaputra River Basin: A Case Study of Shallow Aquifers in Inner Guwahati City, Assam, India, Geographies, 4, 675–686, https://doi.org/10.3390/geographies4040037, number: 4 Publisher: Multidisciplinary Digital Publishing Institute, 2024.

https://doi.org/10.5194/egusphere-2025-5625
Preprint. Discussion started: 20 January 2026

Mehrnegar, N. and Forootan, E.: GRACE and GRACE-FO Post Processing in Matlab (Version 1), https://doi.org/https://doi.org/10.6084/m9.figshare.29929922.v1, 2025.

Mehrnegar, N., Jones, O., Singer, M. B., Schumacher, M., Bates, P., and Forootan, E.: Comparing global hydrological models and combining them with GRACE by dynamic model data averaging (DMDA), Advances in Water Resources, 138, 103 528, https://doi.org/10.1016/j.advwatres.2020.103528, 2020.

Mirza, M. Q.: Three Recent Extreme Floods in Bangladesh: A Hydro-Meteorological Analysis, Natural Hazards, 28, 35–64, https://doi.org/10.1023/A:1021169731325, 2003.

Mitchell, H. L. and Houtekamer, P. L.: An Adaptive Ensemble Kalman Filter, Monthly Weather Review, 128, 416–433, https://doi.org/10.1175/1520-0493(2000)128<0416:AAEKF>2.0.CO;2, publisher: American Meteorological Society Section: Monthly Weather Review, 2000.

Mizukami, N., Clark, M. P., Sampson, K., Nijssen, B., Mao, Y., McMillan, H., Viger, R. J., Markstrom, S. L., Hay, L. E., Woods, R., Arnold, J. R., and Brekke, L. D.: mizuRoute version 1: a river network routing tool for a continental domain water resources applications, Geoscientific Model Development, 9, 2223–2238, https://doi.org/10.5194/gmd-9-2223-2016, publisher: Copernicus GmbH, 2016.

Muñoz Sabater, J. et al.: ERA5-Land hourly data from 1981 to present, Copernicus Climate Change Service (C3S) Climate Data Store (CDS), 10, https://doi.org/10.24381/cds.e2161bac, 2019.

Müller Schmied, H. and Schiebener, L.: The global water resources and use model WaterGAP v2.2e: streamflow calibration and evaluation data basis, https://doi.org/10.5281/zenodo.7255968, 2022.

Müller Schmied, H., Cáceres, D., Eisner, S., Flörke, M., Herbert, C., Niemann, C., Peiris, T. A., Popat, E., Portmann, F. T., Reinecke, R., Schumacher, M., Shadkam, S., Telteu, C.-E., Trautmann, T., and Döll, P.: The global water resources and use model WaterGAP v2.2d: model description and evaluation, Geoscientific Model Development, 14, 1037–1079, https://doi.org/10.5194/gmd-14-1037-2021, publisher: Copernicus GmbH, 2021.

Müller Schmied, H., Trautmann, T., Ackermann, S., Cáceres, D., Flörke, M., Gerdener, H., Kynast, E., Peiris, T. A., Schiebener, L., Schumacher, M., and Döll, P.: The global water resources and use model WaterGAP v2.2e: description and evaluation of modifications and new features, Geoscientific Model Development, 17, 8817–8852, https://doi.org/10.5194/gmd-17-8817-2024, publisher: Copernicus GmbH, 2024.

Nie, Y., Pritchard, H. D., Liu, Q., Hennig, T., Wang, W., Wang, X., Liu, S., Nepal, S., Samyn, D., Hewitt, K., and Chen, X.: Glacial change and hydrological implications in the Himalaya and Karakoram, Nat Rev Earth Environ, 2, 91–106, https://doi.org/10.1038/s43017-020-00124-w, publisher: Nature Publishing Group, 2021.

Nyenah, E., Döll, P., Flörke, M., Mühlenbruch, L., Nissen, L., and Reinecke, R.: The process and value of reprogramming a legacy global hydrological model, Geoscientific Model Development, 18, 5635–5653, https://doi.org/10.5194/gmd-18-5635-2025, publisher: Copernicus GmbH, 2025.

Preimesberger, W., Scanlon, T., Su, C.-H., Gruber, A., and Dorigo, W.: Homogenization of Structural Breaks in the Global ESA CCI Soil Moisture Multisatellite Climate Data Record, IEEE Transactions on Geoscience and Remote Sensing, 59, 2845–2862, https://doi.org/10.1109/TGRS.2020.3012896, 2021.

Rahman, S., Islam, A. K. M. S., Saha, P., Tazkia, A. R., Krien, Y., Durand, F., Testut, L., Islam, G. M. T., and Bala, S. K.: Projected changes of inundation of cyclonic storms in the Ganges–Brahmaputra–Meghna delta of Bangladesh due to SLR by 2100, J Earth Syst Sci, 128, 145, https://doi.org/10.1007/s12040-019-1184-8, 2019.

https://doi.org/10.5194/egusphere-2025-5625
Preprint. Discussion started: 20 January 2026

Rao, M. P., Cook, E. R., Cook, B. I., D'Arrigo, R. D., Palmer, J. G., Lall, U., Woodhouse, C. A., Buckley, B. M., Uriarte, M., Bishop, D. A., Jian, J., and Webster, P. J.: Seven centuries of reconstructed Brahmaputra River discharge demonstrate underestimated high discharge and flood hazard frequency, Nat Commun, 11, 6017, https://doi.org/10.1038/s41467-020-19795-6, 2020.

Reichle, R. H.: Data assimilation methods in the Earth sciences, Advances in water resources, 31, 1411–1418, https://doi.org/10.1016/j.advwatres.2008.01.001, 2008.

Reichle, R. H. and Koster, R. D.: Global assimilation of satellite surface soil moisture retrievals into the NASA Catchment land surface model, Geophysical Research Letters, 32, https://doi.org/10.1029/2004GL021700, 2005.

Renzullo, L. J., van Dijk, A. I. J. M., Perraud, J. M., Collins, D., Henderson, B., Jin, H., Smith, A. B., and McJannet, D. L.: Continental satellite soil moisture data assimilation improves root-zone moisture analysis for water resources assessment, Journal of Hydrology, 519, 2747–2762, https://doi.org/10.1016/j.jhydrol.2014.08.008, 2014.

Retegui-Schiettekatte, L., Schumacher, M., Madsen, H., and Forootan, E.: Assessing daily GRACE Data Assimilation during flood events of the Brahmaputra River Basin, Science of The Total Environment, 975, 179 181, https://doi.org/10.1016/j.scitotenv.2025.179181, 2025a.

Retegui-Schiettekatte, L., Schumacher, M., Yang, F., Madsen, H., and Forootan, E.: An ensemble Kalman filter with rescaling disaggregation for assimilating terrestrial water storage into hydrological models, Sci Rep, 15, 28 675, https://doi.org/10.1038/s41598-025-13602-2, publisher: Nature Publishing Group, 2025b.

RGI Consortium: Randolph Glacier Inventory - A Dataset of Global Glacier Outlines, Version 7, https://doi.org/10.5067/F6JMOVY5NAVZ, 2023.

Ridler, M.-E., Madsen, H., Stisen, S., Bircher, S., and Fensholt, R.: Assimilation of SMOS-derived soil moisture in a fully integrated hydrological and soil-vegetation-atmosphere transfer model in Western Denmark, Water Resources Research, 50, 8962–8981, https://doi.org/10.1002/2014WR015392, 2014.

Sammonds, P., Shamsudduha, M., and Ahmed, B.: Climate change driven disaster risks in Bangladesh and its journey towards resilience, JBA, 9s8, 55–77, https://doi.org/10.5871/jba/009s8.055, 2021.

Schumacher, M.: Methods for assimilating remotely-sensed water storage changes into hydrological models, Thesis, Universitäts- und Landesbibliothek Bonn, https://bonndoc.ulb.uni-bonn.de/xmlui/handle/20.500.11811/6630, accepted: 2020-04-21T14:36:05Z, 2016.

Schumacher, M., Kusche, J., and Döll, P.: A systematic impact assessment of GRACE error correlation on data assimilation in hydrological models, J Geod, 90, 537–559, https://doi.org/10.1007/s00190-016-0892-y, 2016.

Schumacher, M., Forootan, E., van Dijk, A. I. J. M., Müller Schmied, H., Crosbie, R. S., Kusche, J., and Döll, P.: Improving drought simulations within the Murray-Darling Basin by combined calibration/assimilation of GRACE data into the WaterGAP Global Hydrology Model, Remote Sensing of Environment, 204, 212–228, https://doi.org/10.1016/j.rse.2017.10.029, 2018.

Schumacher, M., van Dijk, A. I. J. M., Retegui-Schiettekatte, L., Yang, F., and Forootan, E.: Space-based natural and human-induced water storage change quantification, Sci Rep, 15, 1–10, https://doi.org/10.1038/s41598-025-01938-8, publisher: Nature Publishing Group, 2025.

Shamsudduha, M. and Panda, D. K.: Spatio-temporal changes in terrestrial water storage in the Himalayan river basins and risks to water security in the region: A review, International Journal of Disaster Risk Reduction, 35, 101 068, https://doi.org/10.1016/j.ijdrr.2019.101068, 2019.

Shamsudduha, M., Taylor, R. G., and Longuevergne, L.: Monitoring groundwater storage changes in the highly seasonal humid tropics: Validation of GRACE measurements in the Bengal Basin, Water Resources Research, 48, https://doi.org/10.1029/2011WR010993, _eprint: https://agupubs.onlinelibrary.wiley.com/doi/pdf/10.1029/2011WR010993, 2012.

https://doi.org/10.5194/egusphere-2025-5625
Preprint. Discussion started: 20 January 2026

Shamsudduha, M., Taylor, R. G., Haq, M. I., Nowreen, S., Zahid, A., and Ahmed, K. M. U.: The Bengal Water Machine: Quantified freshwater capture in Bangladesh, Science, 377, 1315–1319, https://doi.org/10.1126/science.abm4730, publisher: American Association for the Advancement of Science, 2022.

Shean, D. E., Bhushan, S., Montesano, P., Rounce, D. R., Arendt, A., and Osmanoglu, B.: A Systematic, Regional Assessment of High Mountain Asia Glacier Mass Balance, Front. Earth Sci., 7, https://doi.org/10.3389/feart.2019.00363, publisher: Frontiers, 2020.

Sherpa, S. F. and Werth, S.: Investigating the Influence of Climate Seasonality on Glacier Mass Changes in High Mountain Asia via GRACE Observations, IEEE Journal of Selected Topics in Applied Earth Observations and Remote Sensing, 18, 20 545–20 562, https://doi.org/10.1109/JSTARS.2025.3595165, 2025.

Siebert, S., Henrich, V., Frenken, K., and Burke, J.: Update of the digital global map of irrigation areas to version 5., https://doi.org/10.13140/2.1.2660.6728, 2013.

Tangdamrongsub, N., Han, S.-C., Yeo, I.-Y., Dong, J., Steele-Dunne, S. C., Willgoose, G., and Walker, J. P.: Multivariate data assimilation of GRACE, SMOS, SMAP measurements for improved regional soil moisture and groundwater storage estimates, Advances in Water Resources, 135, 103 477, https://doi.org/10.1016/j.advwatres.2019.103477, 2020.

Tangdamrongsub, N., Dong, J., and Shellito, P.: Assessing Performances of Multivariate Data Assimilation Algorithms with SMOS, SMAP, and GRACE Observations for Improved Soil Moisture and Groundwater Analyses, Water, 14, 621, https://doi.org/10.3390/w14040621, 2022.

Tapley, B. D., Bettadpur, S., Ries, J. C., Thompson, P. F., and Watkins, M. M.: GRACE measurements of mass variability in the Earth system, Science, 305, 503–505, https://doi.org/10.1126/science.1099192, 2004.

Tian, S., Tregoning, P., Renzullo, L. J., van Dijk, A. I. J. M., Walker, J. P., Pauwels, V. R. N., and Allgeyer, S.: Improved water balance component estimates through joint assimilation of GRACE water storage and SMOS soil moisture retrievals, Water Resources Research, 53, 1820–1840, https://doi.org/10.1002/2016WR019641, 2017.

Uhe, P. F., Mitchell, D. M., Bates, P. D., Sampson, C. C., Smith, A. M., and Islam, A. S.: Enhanced flood risk with 1.5 °C global warming in the Ganges–Brahmaputra–Meghna basin, Environmental Research Letters, 14, 074 031, https://doi.org/10.1088/1748-9326/ab10ee, 2019.

van Dijk, A.: The Australian Water Resources Assessment System. Technical Report 3. Landscape Model (version 0.5) Technical Description. CSIRO: Water for a Healthy Country National Research Flagship., Tech. rep., 2010.

Van Dijk, A. I. J. M.: The Australian Water Resources Assessment System: Technical 901 Report 3, Landscape model (version 0.5) Technical Description, CSIRO, Water for a Healthy Country National Research Flagship, 2010.

van Dijk, A. I. J. M., Peña-Arancibia, J. L., Wood, E. F., Sheffield, J., and Beck, H. E.: Global analysis of seasonal streamflow predictability using an ensemble prediction system and observations from 6192 small catchments worldwide, Water Resources Research, 49, 2729–2746, https://doi.org/10.1002/wrcr.20251, 2013.

Van Dijk, A. I. J. M., Renzullo, L. J., Wada, Y., and Tregoning, P.: A global water cycle reanalysis (2003–2012) merging satellite gravimetry and altimetry observations with a hydrological multi-model ensemble, Hydrology and Earth System Sciences, 18, 2955–2973, https://doi.org/10.5194/hess-18-2955-2014, 2014.

Vicente-Serrano, S. M., Beguería, S., and López-Moreno, J. I.: A Multiscalar Drought Index Sensitive to Global Warming: The Standardized Precipitation Evapotranspiration Index, Journal of Climate, 23, 1696–1718, https://doi.org/10.1175/2009JCLI2909.1, publisher: American Meteorological Society Section: Journal of Climate, 2010.

Vishwakarma, B. D., Ramsankaran, R., Azam, M. F., Bolch, T., Mandal, A., Srivastava, S., Kumar, P., Sahu, R., Navinkumar, P. J., Tanniru, S. R., Javed, A., Soheb, M., Dimri, A. P., Yadav, M., Devaraju, B., Chinnasamy, P., Reddy, M. J., Murugesan, G. P., Arora, M., Jain, S. K.,

https://doi.org/10.5194/egusphere-2025-5625
Preprint. Discussion started: 20 January 2026

Ojha, C. S. P., Harrison, S., and Bamber, J.: Challenges in Understanding the Variability of the Cryosphere in the Himalaya and Its Impact on Regional Water Resources, Front. Water, 4, https://doi.org/10.3389/frwa.2022.909246, publisher: Frontiers, 2022.

Wongchuig, S., Paiva, R., Siqueira, V., Papa, F., Fleischmann, A., Biancamaria, S., Paris, A., Parrens, M., and Al Bitar, A.: Multi-Satellite Data Assimilation for Large-Scale Hydrological-Hydrodynamic Prediction: Proof of Concept in the Amazon Basin, Water Resources Research, 60, e2024WR037 155, https://doi.org/10.1029/2024WR037155, 2024.

Wouters, B., Gardner, A. S., and Moholdt, G.: Global Glacier Mass Loss During the GRACE Satellite Mission (2002-2016), Front. Earth Sci., 7, https://doi.org/10.3389/feart.2019.00096, publisher: Frontiers, 2019.

Wu, W.-Y., Yang, Z.-L., Zhao, L., and Lin, P.: The impact of multi-sensor land data assimilation on river discharge estimation, Remote Sensing of Environment, 279, 113 138, https://doi.org/10.1016/j.rse.2022.113138, 2022.

Yang, F., Forootan, E., Liu, S., and Schumacher, M.: A Monte Carlo Propagation of the Full Variance-Covariance of GRACE-Like Level-2 Data With Applications in Hydrological Data Assimilation and Sea-Level Budget Studies, Water Resources Research, 60, e2023WR036 764, https://doi.org/10.1029/2023WR036764, 2024.

Yang, F., Schumacher, M., Retegui-Schiettekatte, L., van Dijk, A. I. J. M., and Forootan, E.: PyGLDA: a fine-scale python-based global land data assimilation system for integrating satellite gravity data into hydrological models, Geoscientific Model Development, 18, 6195–6217, https://doi.org/10.5194/gmd-18-6195-2025, publisher: Copernicus GmbH, 2025.

Zaitchik, B. F., Rodell, M., and Reichle, R. H.: Assimilation of GRACE Terrestrial Water Storage Data into a Land Surface Model: Results for the Mississippi River Basin, Journal of Hydrometeorology, 9, 535–548, https://doi.org/10.1175/2007JHM951.1, 2008.

Zhao, L. and Yang, Z.-L.: Multi-sensor land data assimilation: Toward a robust global soil moisture and snow estimation, Remote Sensing of Environment, 216, 13–27, https://doi.org/10.1016/j.rse.2018.06.033, 2018.